Geometrical parameterization of the crystal chemistry of P63/m apatites: comparison with experimental data and ab initio results

Mercier, Patrick; Le Page, Yvon; Whitfield, Pamela S.; Mitchell, Lyndon D.; Davidson, Isobel; White, T. J.

Publisher's version / Version de l'éditeur:
https://doi.org/10.1107/S0108768105031125
Acta Crystallographica Section B: Structural Science, Crystal Engineering and Materials, 61, 6, pp. 635-655, 2005-12

Acta Crystallographica Section B
Structural Science
ISSN 0108-7681

Geometrical parameterization of the crystal chemistry of $P6_3/m$ apatites: comparison with experimental data and *ab initio* results

Patrick H. J. Mercier,[a]* Yvon Le Page,[a] Pamela S. Whitfield,[a] Lyndon D. Mitchell,[b] Isobel J. Davidson[a] and T. J. White[c]

[a]Institute for Chemical Process and Environmental Technology (ICPET), National Research Council of Canada, Ottawa, Ontario, Canada K1A 0R6, [b]Institute for Research in Construction (IRC), National Research Council of Canada, Ottawa, Ontario, Canada K1A 0R6, and [c]School of Materials Science and Engineering, Nanyang Technological University, Singapore 639798

Correspondence e-mail: patrick.mercier@nrc-cnrc.gc.ca

Received 12 May 2005
Accepted 29 September 2005

Experimental structure refinements and *ab initio* simulation results for 18 published, fully ordered $P6_3/m$ $(A_4^{\rm I})(A_6^{\rm II})(BO_4)_6X_2$ apatite end-member compositions have been analyzed in terms of a geometric crystal-chemical model that allows the prediction of unit-cell parameters (a and c) and all atom coordinates. To an accuracy of ± 0.025 Å, the magnitude of c was reproduced from crystal-chemical parameters characterizing chains of $\ldots$–$A^{\rm II}$–O3–B–O3–$A^{\rm II}$–$\cdots$ atoms, whereas that of a was determined from those describing $(A^{\rm I}{\rm O}_6)$–$(B{\rm O}_4)$ polyhedral arrangements. The c/a ratio could be predicted to $\pm 0.2\%$ using multi-variable functions based on geometric crystal-chemical model predictions, but could not be ascribed to the adjustment of a single crystal-chemical parameter. The correlations observed between algebraically independent crystal-chemical parameters representing the main observed polyhedral distortions reveal them as the minimum-energy solution to accommodate misfit components within this flexible structure type. For materials with given composition, good agreement (within ± 0.5–2.0%) of *ab initio* crystal-chemical parameters was observed with only those from single-crystal refinements with $R \leq 4.0\%$. Agreement with single-crystal work with $R > 4.0\%$ was not as good, while the scatter with those from Rietveld refinements was considerable. Accordingly, *ab initio* cell data, atomic coordinates and crystal-chemical parameters were reported here for the following compositions awaiting experimental work: $(Zn,Hg)_{10}(PO_4)_6(Cl,F)_2$, $(Ca,Cd)_{10}(VO_4)_6Cl_2$ and $(Ca,Pb,Cd)_{10}(CrO_4)_6Cl_2$.

1. Introduction

Natural and synthetic apatite-type materials have applications in geochronology, catalysis, environmental remediation, bone replacement, dentistry and soil treatment (Elliott, 1994; Kohn *et al.*, 2002). There is considerable variability in the radii and valencies of the cations hosted in apatites. No thorough systematization that would allow predictive crystal chemistry has been attempted previously.

Apatites are conveniently described by the general formula $A_4^{\rm I}A_6^{\rm II}(BO_4)_6X_2$, in connection with the contents of a hexagonal unit cell of the space group $P6_3/m$ (the most common space group for apatites), where $A^{\rm I}$ and $A^{\rm II}$ are distinct crystallographic sites that usually accommodate larger divalent (Ca^{2+}, Sr^{2+}, Pb^{2+}, Ba^{2+} *etc.*), monovalent (Na^+, Li^+ *etc.*) and trivalent (Y^{3+}, La^{3+}, Ce^{3+}, Nd^{3+}, Sm^{3+}, Dy^{3+} *etc.*) cations. B cation sites are filled by smaller 3^+, 4^+, 5^+, 6^+ and 7^+ metals and metalloids (P^{5+}, As^{5+}, V^{5+}, Si^{4+} *etc.*) and the X anion site is occupied by halides (F^-, Cl^-, Br^-, I^-), hydroxyl or oxide ions. The structure is remarkably tolerant to complex chemical

substitutions (Pan & Fleet, 2002), with the charge balance being achieved by coupled cation substitutions or the mixing of monovalent and divalent X-anions, and/or *X*-site vacancies. Atomic ordering can also occur over crystallographically distinct $A^{\rm I}$, $A^{\rm II}$, *B* and/or *X* sites, thereby giving rise to lower-symmetry structure types (*e.g.* $P6_3$, $P112_1/m$, $P112_1/b$ *etc.*). To account for this complexity, an approach based on a simple conceptual framework is desirable in which distortions driven by steric requirements lead to progressively more complex derivative structures.

Apatites can be conceived as being constructed from the following structural units:

(i) a hexagonal (or pseudo-hexagonal) network defining the *ab* plane which consists of face-sharing $A^{\rm I}O_6$ polyhedra stacked along the *c* axis that are corner-connected to BO_4 tetrahedra;

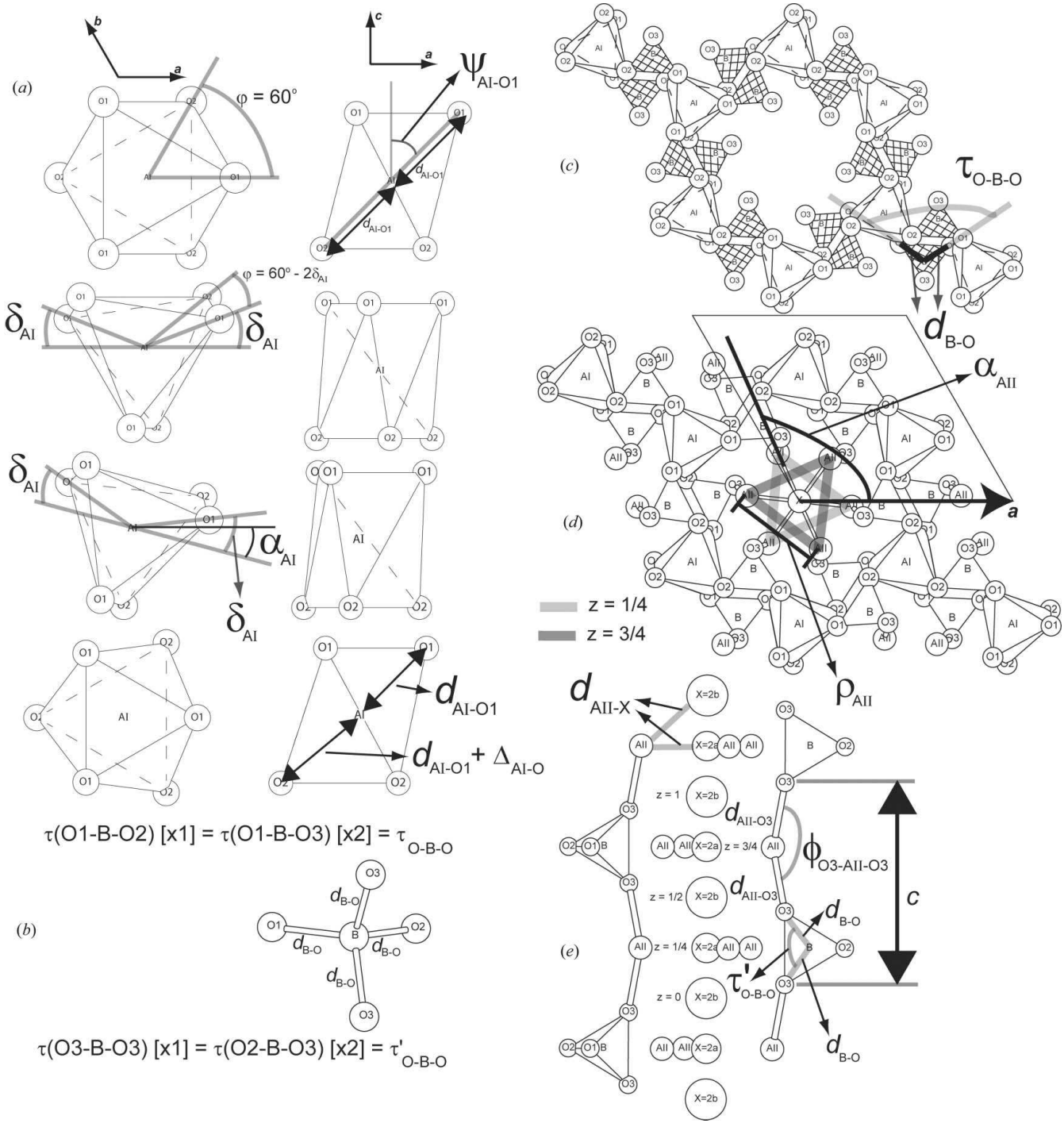

Figure 1
Crystal-chemical parameters used in the geometrical parameterization of $P6_3/m$ apatite. Symbols are as defined in the text and in *Appendix A*.

Table 1
Atomic coordinate data.

(*a*) Fractional atomic coordinates for the geometric crystal-chemical model of $P6_3/m$ apatite

Atom	Multiplicity	Wyckoff letter	x	y	z
$A^{\rm I}$	4	(*f*)	1/3	2/3	0
$A^{\rm II}$	6	(*h*)	$(\rho_{A^{\rm II}}/a)\cdot\{[\cos(\alpha_{A^{\rm II}})/(3^{1/2})] + [\sin(\alpha_{A^{\rm II}})/3]\}$	$[2\cdot\rho_{A^{\rm II}}\cdot\sin(\alpha_{A^{\rm II}})]/[3\cdot a]$	1/4
B	6	(*h*)	$[Bx_{\rm ortho}/a] + [By_{\rm ortho}/(3^{1/2}a)]$	$[2\cdot By_{\rm ortho}/(3^{1/2}a)]$	1/4
O1	6	(*h*)	$(1/3) + [2\cdot d_{A^{\rm I}-{\rm O1}}\cdot\sin(\psi_{A^{\rm I}-{\rm O1}})\cdot\sin(\alpha_{A^{\rm I}} + \delta_{A^{\rm I}})]/[3^{1/2}\cdot a]$ $[\equiv x({\rm O1})]$	$(2/3) + d_{A^{\rm I}-{\rm O1}}\cdot\sin(\psi_{A^{\rm I}-{\rm O1}})\cdot[\sin(\alpha_{A^{\rm I}} + \delta_{A^{\rm I}}) - 3^{1/2}\cdot\cos(\alpha_{A^{\rm I}} + \delta_{A^{\rm I}})]/[3^{1/2}\cdot a]$ $[\equiv y({\rm O1})]$	1/4
O2	6	(*h*)	$(2/3) - (d_{A^{\rm I}-{\rm O1}} + \Delta_{A^{\rm I}-{\rm O}})\cdot\{1 - [\cos^2(\psi_{A^{\rm I}-{\rm O1}})]/[1 + (\Delta_{A^{\rm I}-{\rm O}}/d_{A^{\rm I}-{\rm O1}})]^2\}^{1/2}\cdot[3^{1/2}\cdot\cos(\alpha_{A^{\rm I}} - \delta_{A^{\rm I}}) + \sin(\alpha_{A^{\rm I}} - \delta_{A^{\rm I}})]/[3^{1/2}\cdot a]$ $[\equiv x({\rm O2})]$	$(1/3) - 2\cdot(d_{A^{\rm I}-{\rm O1}} + \Delta_{A^{\rm I}-{\rm O}})\cdot\{1 - [\cos^2(\psi_{A^{\rm I}-{\rm O1}})]/[1 + (\Delta_{A^{\rm I}-{\rm O1}}/d_{A^{\rm I}-{\rm O1}})]^2\}^{1/2}\cdot\sin(\alpha_{A^{\rm I}} - \delta_{A^{\rm I}})/[3^{1/2}\cdot a]$ $[\equiv y({\rm O2})]$	1/4
O3	12	(*i*)	$[{\rm O3}x_{\rm ortho}/a] + [{\rm O3}y_{\rm ortho}/(3^{1/2}a)]$	$[2\cdot{\rm O3}y_{\rm ortho}/(3^{1/2}a)]$	$(1/4)\cdot[d_{B-{\rm O}}\sin(\tau'_{{\rm O}-B-{\rm O}}/2)]/c$
X	2	(*a*) or (*b*)	0	0	1/4, 3/4 (2*a*) or 0, 1/2 (2*b*)

Notes:
(1) $a = 3^{1/2}\cdot\{d_{A^{\rm I}-{\rm O1}}{}^2 - (1/4)\cdot[d_{B-{\rm O}}\cdot\sin(\tau'_{{\rm O}-B-{\rm O}}/2) + d_{A^{\rm II}-{\rm O3}}\cdot\sin(\phi_{{\rm O3}-A^{\rm II}-{\rm O3}}/2)]^2\}^{1/2}\cdot\cos[(\pi/6) - \delta_{A^{\rm I}} - \alpha_{A^{\rm I}}] + 3^{1/2}\cdot\{(d_{A^{\rm I}-{\rm O1}} + \Delta_{A^{\rm I}-{\rm O}})^2 - (1/4)\cdot[d_{B-{\rm O}}\cdot\sin(\tau'_{{\rm O}-B-{\rm O}}/2) + d_{A^{\rm II}-{\rm O3}}\cdot\sin(\phi_{{\rm O3}-A^{\rm II}-{\rm O3}}/2)]^2\}^{1/2}\cdot\cos[(\pi/6) - \delta_{A^{\rm I}} + \alpha_{A^{\rm I}}] + 2\cdot(3^{1/2})\cdot d_{B-{\rm O}}\cdot\sin(\tau_{{\rm O}-B-{\rm O}}/2)\cdot\cos(\theta)$, where $\sin(\theta) = \{\{d_{A^{\rm I}-{\rm O1}}{}^2 - (1/4)\cdot[d_{B-{\rm O}}\cdot\sin(\tau'_{{\rm O}-B-{\rm O}}/2) + d_{A^{\rm II}-{\rm O3}}\cdot\sin(\phi_{{\rm O3}-A^{\rm II}-{\rm O3}}/2)]^2\}^{1/2}\cdot\sin[(\pi/6) - \delta_{A^{\rm I}} - \alpha_{A^{\rm I}}] - \{(d_{A^{\rm I}-{\rm O1}} + \Delta_{A^{\rm I}-{\rm O}})^2 - (1/4)\cdot[d_{B-{\rm O}}\cdot\sin(\tau'_{{\rm O}-B-{\rm O}}/2) + d_{A^{\rm II}-{\rm O3}}\cdot\sin(\phi_{{\rm O3}-A^{\rm II}-{\rm O3}}/2)]^2\}^{1/2}\cdot\sin[(\pi/6) - \delta_{A^{\rm I}} + \alpha_{A^{\rm I}}]\}/[2\cdot d_{B-{\rm O}}\cdot\sin(\tau_{{\rm O}-B-{\rm O}}/2)]$.
(2) $\cos(\psi_{A^{\rm I}-{\rm O1}}) = [d_{B-{\rm O}}\sin(\tau'_{{\rm O}-B-{\rm O}}/2) + d_{A^{\rm II}-{\rm O3}}\sin(\phi_{{\rm O3}-A^{\rm II}-{\rm O3}}/2)]/[2\cdot d_{A^{\rm I}-{\rm O1}}]$.
(3) $c = 2\cdot[d_{B-{\rm O}}\sin(\tau'_{{\rm O}-B-{\rm O}}/2) + d_{A^{\rm II}-{\rm O3}}\sin(\phi_{{\rm O3}-A^{\rm II}-{\rm O3}}/2)]$.
(4) $\tau'_{{\rm O}-B-{\rm O}} = 2\arcsin\{(3^{1/2}/2)\cos[\tau_{{\rm O}-B-{\rm O}} - (\pi/2)]\}$.
(5) For X in 2(*a*): $\rho_{A^{\rm II}} = 3^{1/2}\cdot d_{A^{\rm II}-X}$; for X in 2(*b*): $\rho_{A^{\rm II}} = 3^{1/2}\cdot[d^2_{A^{\rm II}-X} - (c^2/16)]^{1/2}$.
(6) $Bx_{\rm ortho} = a\cdot[x({\rm O2}) - (1/2)\cdot y({\rm O2})] - d_{B-{\rm O}}\cdot\cos[(\pi - \tau_{{\rm O}-B-{\rm O}})/2 + \eta]$; $By_{\rm ortho} = a\cdot[3^{1/2}\cdot y({\rm O2})]/2 - d_{B-{\rm O}}\cdot\sin[(\pi - \tau_{{\rm O}-B-{\rm O}})/2 + \eta]$.
(7) ${\rm O3}x_{\rm ortho} = a\cdot[x({\rm O2}) - (1/2)\cdot y({\rm O2})] - (3/2)\cdot d_{B-{\rm O}}\cdot\cos[\tau_{{\rm O}-B-{\rm O}} - (\pi/2)]\cdot\cos[(\tau_{{\rm O}-B-{\rm O}}/2) + \eta]$; ${\rm O3}y_{\rm ortho} = a\cdot[3^{1/2}\cdot y({\rm O2})]/2 - (3/2)\cdot d_{B-{\rm O}}\cdot\cos[\tau_{{\rm O}-B-{\rm O}} - (\pi/2)]\cdot\sin[(\tau_{{\rm O}-B-{\rm O}}/2) + \eta]$.
(8) $\tan(\eta) = [{\rm O1}y_{\rm ortho} - {\rm O2}y_{\rm ortho}]/[{\rm O1}x_{\rm ortho} - {\rm O2}x_{\rm ortho}]$, where ${\rm O1}x_{\rm ortho} = a\cdot[x({\rm O1}) - (1/2)\cdot y({\rm O1})]$; ${\rm O1}y_{\rm ortho} = a\cdot[3^{1/2}\cdot y({\rm O1})]/2$; ${\rm O2}x_{\rm ortho} = a\cdot[x({\rm O2}) - (1/2)\cdot y({\rm O2})]$; ${\rm O2}y_{\rm ortho} = a\cdot[3^{1/2}\cdot y({\rm O2})]/2$.

(*b*) Extraction of the crystal-chemical parameters from the crystallographic description (*a*, *c*, atom coordinates).

Crystal-chemical parameter	Equations used to calculate the crystal-chemical parameters listed in the first column		
$(A^{\rm I}-{\rm O1})$	$= \{[({\rm O1}x - 1/3)^2 + ({\rm O1}y - 2/3)^2 - ({\rm O1}x - 1/3)\cdot({\rm O1}y - 2/3)]\cdot a^2 + [1/4 - A^{\rm I}z]^2\cdot c^2\}^{1/2}$		
$(A^{\rm I}-{\rm O1})^{A^{\rm I}z=0}$	$= \{[({\rm O1}x - 1/3)^2 + ({\rm O1}y - 2/3)^2 - ({\rm O1}x - 1/3)\cdot({\rm O1}y - 2/3)]\cdot a^2 + (1/16)\cdot c^2\}^{1/2}$		
$\Delta_{A^{\rm I}-{\rm O}}$	$= [(A^{\rm I}-{\rm O2}) - (A^{\rm I}-{\rm O1})]$, where $(A^{\rm I}-{\rm O2}) = \{[({\rm O2}x - 2/3)^2 + ({\rm O2}y - 1/3)^2 - ({\rm O2}x - 2/3)\cdot({\rm O2}y - 1/3)]\cdot a^2 + (A^{\rm I}z + 1/4)^2\cdot c^2\}^{1/2}$		
$\Delta^{A^{\rm I}z=0}_{A^{\rm I}-{\rm O}}$	$= [(A^{\rm I}-{\rm O2})^{A^{\rm I}z=0} - (A^{\rm I}-{\rm O1})^{A^{\rm I}z=0}]$, where $(A^{\rm I}-{\rm O2})^{A^{\rm I}z=0} = \{[({\rm O2}x - 2/3)^2 + ({\rm O2}y - 1/3)^2 - ({\rm O2}x - 2/3)\cdot({\rm O2}y - 1/3)]\cdot a^2 + (1/16)\cdot c^2\}^{1/2}$		
$\psi_{A^{\rm I}-{\rm O1}}$	$= \arcsin\{a\cdot[({\rm O1}x - 1/3)^2 + ({\rm O1}y - 2/3)^2 - ({\rm O1}x - 1/3)\cdot({\rm O1}y - 2/3)]^{1/2}/(A^{\rm I}-{\rm O1})\}$		
$\psi^{A^{\rm I}z=0}_{A^{\rm I}-{\rm O1}}$	$= \arcsin\{a\cdot[({\rm O1}x - 1/3)^2 + ({\rm O1}y - 2/3)^2 - ({\rm O1}x - 1/3)\cdot({\rm O1}y - 2/3)]^{1/2}/(A^{\rm I}-{\rm O1})^{A^{\rm I}z=0}\}$		
$\delta_{A^{\rm I}}$	$= 1/2\cdot[(\pi/3) - \theta1 + \theta2]$,	where	$\cos(\theta1) = [({\rm O1}x - 1/3) - 1/2\cdot({\rm O1}y - 2/3)]/[({\rm O1}x - 1/3)^2 + ({\rm O1}y - 2/3)^2 - ({\rm O1}x - 1/3)\cdot({\rm O1}y - 2/3)]^{1/2}$
$\alpha_{A^{\rm I}}$	$= (\pi/3) - \delta_{A^{\rm I}} + \theta1 = \delta_{A^{\rm I}} - \theta2$		$\cos(\theta2) = [(2/3 - {\rm O2}x) + 1/2\cdot({\rm O2}y - 1/3)]/[({\rm O2}x - 2/3)^2 + ({\rm O2}y - 1/3)^2 - ({\rm O2}x - 2/3)\cdot({\rm O2}y - 1/3)]^{1/2}$
$\varphi_{A^{\rm I}}$	$= (\pi/3) - 2\cdot\delta_{A^{\rm I}}$		
$\langle B-{\rm O}\rangle$	$= 1/4\cdot[(B-{\rm O1}) + (B-{\rm O2}) + 2\cdot(B-{\rm O3})]$	where	$(B-{\rm O1}) = \{[(Bx - {\rm O1}x)^2 + (By - {\rm O1}y)^2 - (Bx - {\rm O1}x)\cdot(By - {\rm O1}y)]\cdot a^2\}^{1/2}$ $(B-{\rm O2}) = \{[(Bx - {\rm O2}x)^2 + (By - {\rm O2}y)^2 - (Bx - {\rm O2}x)\cdot(By - {\rm O2}y)]\cdot a^2\}^{1/2}$, $(B-{\rm O3}) = \{[(Bx - {\rm O3}x)^2 + (By - {\rm O3}y)^2 - (Bx - {\rm O3}x)\cdot(By - {\rm O3}y)]\cdot a^2 + (1/4 - {\rm O3}z)^2\cdot c^2\}^{1/2}$
$\langle\tau_{{\rm O}-B-{\rm O}}\rangle$	$= 1/3\cdot[\tau({\rm O1}-B-{\rm O2}) + 2\cdot\tau({\rm O1}-B-{\rm O3})]$	where	$\cos[\tau({\rm O1}-B-{\rm O2})] = a^2\cdot\{({\rm O1}x - Bx)\cdot({\rm O2}x - Bx) + ({\rm O1}y - By)\cdot({\rm O2}y - By) - 1/2\cdot[({\rm O1}x - Bx)\cdot({\rm O2}y - By) + ({\rm O1}y - By)\cdot({\rm O2}x - Bx)]\}/[(B-{\rm O1})\cdot(B-{\rm O2})]$ $\cos[\tau({\rm O1}-B-{\rm O3})] = a^2\cdot\{({\rm O1}x - Bx)\cdot({\rm O3}x - Bx) + ({\rm O1}y - By)\cdot({\rm O3}y - By) - 1/2\cdot[({\rm O1}x - Bx)\cdot({\rm O3}y - By) + ({\rm O1}y - By)\cdot({\rm O3}x - Bx)]\}/[(B-{\rm O1})\cdot(B-{\rm O3})]$
$\rho_{A^{\rm II}}$	$= a\cdot[(A^{\rm II}x + A^{\rm II}y)^2 + (2\cdot A^{\rm II}y - A^{\rm II}x)^2 - (A^{\rm II}x + A^{\rm II}y)\cdot(2\cdot A^{\rm II}y - A^{\rm II}x)]^{1/2}$		
$(A^{\rm II}-X)$	$= [(A^{\rm II}x^2 + A^{\rm II}y^2 - A^{\rm II}x\cdot A^{\rm II}y)\cdot a^2 + (Xz - 1/4)^2\cdot c^2]^{1/2}$		
$\alpha_{A^{\rm II}}$	$= \arccos[3^{1/2}\cdot a\cdot(A^{\rm II}x - 1/2\cdot A^{\rm II}y)/\rho_{A^{\rm II}}]$		
$(A^{\rm II}-{\rm O3})$	$= \{[(A^{\rm II}x - {\rm O3}x + {\rm O3}y)^2 + (A^{\rm II}y - {\rm O3}x)^2 - (A^{\rm II}x - {\rm O3}x + {\rm O3}y)\cdot(A^{\rm II}y - {\rm O3}x)]\cdot a^2 + [1/4 + {\rm O3}z]^2\cdot c^2\}^{1/2}$		
$\phi_{{\rm O3}-A^{\rm II}-{\rm O3}}$	$= \pi - 2\arcsin\{a\cdot[(A^{\rm II}x - {\rm O3}x + {\rm O3}y)^2 + (A^{\rm II}y - {\rm O3}x)^2 - (A^{\rm II}x - {\rm O3}x + {\rm O3}y)\cdot(A^{\rm II}y - {\rm O3}x)]^{1/2}/(A^{\rm II}-{\rm O3})\}$		

Notes: (1) The symbols a, c and $A^{\rm I}z$, $A^{\rm II}x$, $A^{\rm II}y$, Bx, By, ${\rm O1}x$, ${\rm O1}y$, ${\rm O2}x$, ${\rm O2}y$, ${\rm O3}x$, ${\rm O3}y$, ${\rm O3}z$, Xz refer to the unit-cell parameters and fractional atom coordinates, respectively. (2) The equations provided are based on standard crystallographic computations of bond lengths and bond angles. (3) The angles $\theta1$ and $\theta2$ referred to in this table are shown in Fig. 9*a* (*Appendix A*).

Table 2
Unit-cell parameters (a and c) and atom coordinates obtained by experimental structure refinements and coordinate-only (CO) or cell-and-coordinate (CC) *ab initio* optimizations.

(a)

Label No.	Composition	Type	R (%)	E_{total} (eV per unit cell)	a (Å)	c (Å)	$A^{I}z$	$A^{II}x$	$A^{II}y$	Bx
1	$Ca_{10}(PO_4)_6F_2$	Single *Xtal*	2.50	–	9.375	6.887	−0.0011	0.00721	0.24875	0.39785
2	$Ca_{10}(PO_4)_6F_2$	Rietveld	–	–	9.3642	6.8811	−0.0018	0.007	0.249	0.3993
3	$Ca_{10}(PO_4)_6F_2$	Single *Xtal*	2.50	–	9.3917	6.8826	−0.00112	0.00712	0.24898	0.39845
4	$Ca_{10}(PO_4)_6F_2$	Single *Xtal*	2.30	–	9.3718	6.8876	−0.00106	0.0071	0.24865	0.39809
5	$Ca_{10}(PO_4)_6F_2$	Single *Xtal*	4.40	–	9.369	6.8839	−0.0013	0.0074	0.2491	0.3978
6	$Ca_{10}(PO_4)_6F_2$	Single *Xtal*	1.60	–	9.3666	6.8839	−0.0011	0.0071	0.2487	0.3981
7	$Ca_{10}(PO_4)_6F_2$	Single *Xtal*	2.90	–	9.363	6.878	−0.0012	0.0071	0.2486	0.3982
8	$Ca_{10}(PO_4)_6F_2$	Single *Xtal*	1.60	–	9.367	6.884	−0.0011	0.0071	0.2487	0.3981
101	$Ca_{10}(PO_4)_6F_2$	CO	–	−303.035	9.367	6.884	0.00093	0.00603	0.24746	0.39759
102	$Ca_{10}(PO_4)_6F_2$	CO	–	−303.052	9.375	6.887	0.00097	0.00582	0.24738	0.39760
103	$Ca_{10}(PO_4)_6F_2$	CC	–	−303.113	9.30074	6.85123	0.00039	0.00760	0.24777	0.39801
9	$Ca_{10}(PO_4)_6Br_2$	Single *Xtal*	3.08	–	9.761	6.739	0.0045	−0.0121	0.2551	0.4124
104	$Ca_{10}(PO_4)_6Br_2$	CO	–	−296.112	9.761	6.739	0.00440	−0.01581	0.25172	0.41216
105	$Ca_{10}(PO_4)_6Br_2$	CC	–	−296.153	9.72524	6.69531	0.00444	−0.01485	0.25160	0.41217
10	$Pb_{10}(PO_4)_6Cl_2$	Single *Xtal*	5.20	–	9.9981	7.344	0.0051	−0.006	0.2487	0.4102
11	$Pb_{10}(PO_4)_6Cl_2$	Single *Xtal*	2.10	–	9.9764	7.3511	0.0048	−0.00536	0.24893	0.4104
12	$Pb_{10}(PO_4)_6Cl_2$	Single *Xtal*	5.80	–	9.993	7.334	0.0051	−0.006	0.2487	0.4102
13	$Pb_{10}(PO_4)_6Cl_2$	Rietveld	–	–	9.9767	7.3255	0.0047	−0.0047	0.2501	N/A
106	$Pb_{10}(PO_4)_6Cl_2$	CO	–	−270.056	9.9981	7.344	−0.00352	−0.00442	0.24722	0.40780
107	$Pb_{10}(PO_4)_6Cl_2$	CC	–	−270.046	9.96556	7.29404	0.00347	−0.00362	0.24701	0.40704
14	$Pb_{10}(PO_4)_6Br_2$	Rietveld	–	–	10.0218	7.3592	0.0067	−0.0053	0.2565	N/A
108	$Pb_{10}(PO_4)_6Br_2$	CO	–	−268.573	10.0618	7.3592	0.00437	−0.00594	0.25240	0.40906
109	$Pb_{10}(PO_4)_6Br_2$	CC	–	−268.597	10.05212	7.30715	0.00417	−0.00425	0.25328	0.40898
15	$Pb_{10}(PO_4)_6F_2$	Rietveld	–	–	9.7547	7.2832	0.0031	−0.0022	0.2302	N/A
16	$Pb_{10}(PO_4)_6F_2$	Single *Xtal*	4.90		9.76	7.3	0.0029	−0.0026	0.2376	0.4004
110	$Pb_{10}(PO_4)_6F_2$	CO	–	−272.892	9.76	7.3	0.00155	0.00846	0.25178	0.39958
111	$Pb_{10}(PO_4)_6F_2$	CC	–	−272.952	9.80940	7.34066	0.00158	0.00681	0.25099	0.39935
112	$Pb_{10}(PO_4)_6F_2$	CO	–	−272.902	9.76	7.3	0.00140	0.00886	0.25199	0.40095
17	$Cd_{10}(PO_4)_6Cl_2$	Single *Xtal*	5.60		9.633	6.484	0.0054	−0.0188	0.2534	0.4047
18	$Cd_{10}(PO_4)_6Cl_2$	Single *Xtal*	7.50		9.625	6.504	0.0044	−0.0141	0.2537	0.4035
113	$Cd_{10}(PO_4)_6Cl_2$	CO	–	−234.875	9.633	6.484	−0.00006	−0.01868	0.25076	0.40287
114	$Cd_{10}(PO_4)_6Cl_2$	CC	–	−234.289	9.79420	6.52950	−0.01553	−0.01797	0.25681	0.40248
115	$Cd_{10}(PO_4)_6Cl_2$	CO	–	−236.162	9.625	6.504	0.00310	−0.01666	0.24205	0.40420
116	$Cd_{10}(PO_4)_6Cl_2$	CC	–	−236.221	9.68224	6.44006	0.00307	−0.02117	0.23868	0.40603
19	$Pb_{10}(AsO_4)_6Cl_2$	Single *Xtal*	2.70	–	10.211	7.4185	0.007	−0.0045	0.24652	0.4095
20	$Pb_{10}(AsO_4)_6Cl_2$	Single *Xtal*	3.10	–	10.211	7.4185	0.007	−0.0047	0.2464	0.4091
21	$Pb_{10}(AsO_4)_6Cl_2$	Single *Xtal*	5.70		10.25	7.454	0.0065	−0.0042	0.2472	0.4096
117	$Pb_{10}(AsO_4)_6Cl_2$	CO	–	−243.189	10.211	7.4185	0.00358	−0.00612	0.24190	0.40551
118	$Pb_{10}(AsO_4)_6Cl_2$	CC	–	−243.192	10.24461	7.37367	0.00378	−0.00855	0.24062	0.40629
22	$Ca_4Pb_6(AsO_4)_6\ Cl_2$	Single *Xtal*	6.20	–	10.14	7.185	0.009	−0.0142	0.2439	0.4021
119	$Ca_4Pb_6(AsO_4)_6\ Cl_2$	CO	–	−254.488	10.14	7.185	0.00578	−0.01761	0.23802	0.41976
120	$Ca_4Pb_6(AsO_4)_6\ Cl_2$	CC	–	−254.514	10.14861	7.121656	0.00574	−0.01817	0.23734	0.42016
23	$Sr_{10}(PO_4)_6Cl_2$	Single *Xtal*	3.40	–	9.859	7.206	0.0009	0.0104	0.2592	0.4052
24	$Sr_{10}(PO_4)_6Cl_2$	Rietveld	–	–	9.8774	7.189	0.0011	0.0097	0.2583	0.4005
25	$Sr_{10}(PO_4)_6Cl_2$	Rietveld	–	–	9.8777	7.1892	0	0.0073	0.2561	0.4054
121	$Sr_{10}(PO_4)_6Cl_2$	CO	–	−295.014	9.859	7.206	0.00087	0.00970	0.25671	0.40557
122	$Sr_{10}(PO_4)_6Cl_2$	CC	–	−295.037	9.83822	7.16706	0.00091	0.00947	0.25585	0.40582
26	$Sr_{10}(PO_4)_6Br_2$	Rietveld	–	–	9.9641	7.207	−0.0022	0.0117	0.2642	0.4082
27	$Sr_{10}(PO_4)_6Br_2$	Single *Xtal*	5.20	–	9.972	7.214	0.00163	0.00878	0.26428	0.4087
123	$Sr_{10}(PO_4)_6Br_2$	CO	–	−293.271	9.972	7.214	0.00150	0.00732	0.26236	0.40796
124	$Sr_{10}(PO_4)_6Br_2$	CC	–	−293.306	9.92739	7.18399	0.00160	0.00865	0.26231	0.40786
29	$(Sr_{0.992}Nd_{0.005})_{10}(PO_4)_6F_2$	Single *Xtal*	2.30	–	9.7156	7.281	−0.0002	0.01445	0.25355	0.3992
125	$Sr_{10}(PO_4)_6F_2$	CO	–	−299.539	9.718	7.288	−0.00064	0.01467	0.25426	0.39985
126	$Sr_{10}(PO_4)_6F_2$	CO	–	−299.509	9.7156	7.281	−0.00024	0.01420	0.25400	0.39912
127	$Sr_{10}(PO_4)_6F_2$	CC	–	−299.547	9.67197	7.24993	−0.00025	0.01526	0.25427	0.39924
30	$(Sr_{0.982}Nd_{0.012})_{10}(VO_4)_6F_2$	Single *Xtal*	2.20	–	10.0077	7.4342	0.0004	0.0106	0.24944	0.3982
128	$Sr_{10}(VO_4)_6F_2$	CO	–	−319.161	10.0077	7.4342	0.00066	0.00981	0.24894	0.39850
129	$Sr_{10}(VO_4)_6F_2$	CC	–	−319.229	9.94173	7.39979	0.00076	0.01115	0.24919	0.39861
31	$Sr_{10}(VO_4)_6CuO$	Single *Xtal*	6.70	–	10.126	7.415	0.0015	0.00952	0.25944	0.4003
130	$Sr_{10}(VO_4)_6CuO$	CO	–	−327.534	10.126	7.415	−0.00158	0.00918	0.25990	0.40032
131	$Sr_{10}(VO_4)_6CuO$	CC	–	−327.582	10.06833	7.38539	−0.00164	0.01069	0.26044	0.40021
132	$Ba_{10}(PO_4)_6F_2$	CO	–	−299.866	10.153	7.733	−0.00129	0.01682	0.24440	0.40222
	$Ba_{10}(PO_4)_6F_2$	Single *Xtal*	–	–	10.153	7.733	Disordered X site (Mathew *et al.*, 1979)			
32	$Ba_{10}(PO_4)_6Br_2$	Single *Xtal*	3.28	–	10.342	7.673	0.00123	0.01588	0.26763	0.4085
133	$Ba_{10}(PO_4)_6Br_2$	CO	–	−294.796	10.342	7.673	0.00148	0.01616	0.26602	0.40699
134	$Ba_{10}(PO_4)_6Br_2$	CC	–	−294.800	10.31411	7.67383	0.00151	0.01704	0.26617	0.40708
33	$Ba_{10}(PO_4)_6Cl_2$	Single *Xtal*	3.40	–	10.284	7.651	0.0007	0.0157	0.2606	0.4064

Table 2 (continued)

Label No.	Composition	Type	R (%)	E_{total} (eV per unit cell)	a (Å)	c (Å)	$A^{I}z$	$A^{II}x$	$A^{II}y$	Bx
135	$Ba_{10}(PO_4)_6Cl_2$	CO	–	−296.501	10.284	7.651	0.00056	0.01570	0.25925	0.40550
136	$Ba_{10}(PO_4)_6Cl_2$	CO	–	−296.503	10.284	7.651	0.00028	0.01525	0.25863	0.40544
137	$Ba_{10}(PO_4)_6Cl_2$	CC	–	−296.513	10.25489	7.64122	0.00076	0.01617	0.25857	0.40551
34	$Ba_{10}(MnO_4)_6F_2$	Cell parameters (Dardenne *et al.*, 1999)	–	–	10.3437	7.8639	–	–	–	–
138	$Ba_{10}(MnO_4)_6F_2$	CO	–	−295.790	10.3437	7.8639	−0.00133	0.01754	0.25641	0.40083
139	$Ba_{10}(MnO_4)_6F_2$	CC	–	−295.830	10.29782	7.830865	−0.00125	0.01837	0.25649	0.40103
140	$Ba_{10}(MnO_4)_6F_2$	CO	–	−295.136	10.3437	7.8639	−0.00277	0.01213	0.23985	0.40181
141	$Ba_{10}(MnO_4)_6F_2$	CC	–	−295.516	10.22853	7.70059	−0.00288	0.01368	0.23651	0.40275
35	$Pb_{10}(VO_4)_6Cl_2$	Single *Xtal*	2.20	–	10.3174	7.3378	0.0077	−0.01209	0.24275	0.4097
36	$Pb_{10}(VO_4)_6Cl_2$	Single *Xtal*	11.50	–	10.331	7.343	0.0054	−0.0107	0.2451	0.4046
142	$Pb_{10}(VO_4)_6Cl_2$	CO	–	−291.537	10.3174	7.3378	0.00675	−0.01472	0.23910	0.40829
143	$Pb_{10}(VO_4)_6Cl_2$	CC	–	−291.564	10.30221	7.28418	0.00606	−0.01380	0.23908	0.40824

(*b*)

Label No.	Ref.	By	O1x	O1y	O2x	O2y	O3x	O3y	O3z	Xz
1	(*a*)	0.36853	0.3267	0.4844	0.5873	0.4666	0.3416	0.2572	0.0705	0.25
2	(*b*)	0.3693	0.3265	0.4864	0.5886	0.4672	0.3407	0.2561	0.0676	0.25
3	(*c*)	0.36896	0.32694	0.48444	0.5876	0.4665	0.3411	0.2571	0.07076	0.25
4	(*c*)	0.36879	0.32629	0.48435	0.5878	0.46664	0.34067	0.2564	0.07089	0.25
5	(*d*)	0.3685	0.3264	0.4859	0.589	0.4669	0.3421	0.2575	0.0705	0.25
6	(*e*)	0.3688	0.3262	0.4843	0.588	0.4668	0.3416	0.2568	0.0704	0.25
7	(*f*)	0.3689	0.3268	0.485	0.5881	0.4668	0.3415	0.2569	0.0704	0.25
8	(*f*)	0.3688	0.3262	0.4843	0.588	0.4668	0.3416	0.2568	0.0704	0.25
101	(*g*)	0.36780	0.32445	0.48403	0.58976	0.46788	0.34079	0.25436	0.06880	0.25
102	(*g*)	0.36784	0.32463	0.48409	0.58968	0.46778	0.34080	0.25446	0.06885	0.25
103	(*g*)	0.36829	0.32392	0.48468	0.59109	0.46904	0.34073	0.25398	0.06802	0.25
9	(*h*)	0.3785	0.3533	0.4972	0.5954	0.4642	0.3572	0.2713	0.0662	0
104	(*g*)	0.37829	0.35276	0.49841	0.59741	0.46459	0.35684	0.26934	0.06401	0
105	(*g*)	0.37809	0.35176	0.49783	0.59784	0.46528	0.35701	0.26869	0.06322	0
10	(*i*)	0.3790	0.3402	0.4893	0.5871	0.4735	0.3593	0.2738	0.0848	0
11	(*j*)	0.3787	0.3430	0.4900	0.5900	0.4750	0.3590	0.2740	0.0840	0
12	(*k*)	0.3790	0.3402	0.4893	0.5871	0.4735	0.3593	0.2738	0.0848	0
13	(*l*)	The atoms of BO_4 tetrahedra were considered as a rigid body								
106	(*g*)	0.37574	0.33738	0.48312	0.58965	0.47377	0.35898	0.26918	0.07883	0
107	(*g*)	0.37564	0.33507	0.48238	0.58887	0.47452	0.35858	0.26900	0.07782	0
14	(*l*)	The atoms of BO_4 tetrahedra were considered as a rigid body								
108	(*g*)	0.37468	0.34249	0.48439	0.59022	0.46967	0.36023	0.26928	0.07889	0
109	(*g*)	0.37440	0.34145	0.48332	0.59002	0.46985	0.36060	0.26887	0.07794	0
15	(*l*)	The atoms of BO_4 tetrahedra were considered as a rigid body								
16	(*m*)	0.3813	0.323	0.487	0.582	0.486	0.347	0.267	0.078	0.25
110	(*g*)	0.36958	0.33282	0.48374	0.58437	0.46725	0.34476	0.25947	0.07887	0.25
111	(*g*)	0.36930	0.33312	0.48368	0.58373	0.46643	0.34476	0.26043	0.07954	0.25
112	(*g*)	0.36928	0.33366	0.48294	0.58584	0.46748	0.34695	0.25999	0.07853	0.25
17	(*n*)	0.3773	0.3512	0.5021	0.5909	0.4598	0.3442	0.2667	0.0598	0.25
18	(*o*)	0.3762	0.3462	0.5016	0.5882	0.4589	0.3438	0.261	0.0631	0.25
113	(*g*)	0.39208	0.39290	0.54739	0.58770	0.45442	0.32219	0.28059	0.06394	0.25
114	(*g*)	0.39496	0.39150	0.54673	0.58329	0.45502	0.31921	0.28658	0.06415	0.25
115	(*g*)	0.37746	0.34237	0.49732	0.59282	0.46486	0.34720	0.26501	0.05924	0
116	(*g*)	0.37939	0.34653	0.49988	0.59343	0.46450	0.34814	0.26701	0.05765	0
19	(*p*)	0.3843	0.322	0.494	0.598	0.485	0.358	0.268	0.075	0
20	(*p*)	0.3837	0.328	0.495	0.604	0.486	0.359	0.275	0.067	0
21	(*q*)	0.385	0.329	0.4937	0.5982	0.4872	0.3597	0.2716	0.0733	0
117	(*g*)	0.37867	0.32469	0.49064	0.60112	0.48443	0.35626	0.26203	0.06511	0
118	(*g*)	0.38008	0.32639	0.49232	0.60102	0.48495	0.35711	0.26301	0.06464	0
22	(*r*)	0.3895	0.364	0.523	0.616	0.474	0.365	0.276	0.065	0
119	(*g*)	0.38927	0.36166	0.51996	0.61692	0.47160	0.36254	0.27131	0.05904	0
120	(*g*)	0.38957	0.36182	0.51976	0.61702	0.47190	0.36292	0.27129	0.05766	0
23	(*s*)	0.372	0.3365	0.4821	0.5861	0.4662	0.3549	0.267	0.0768	0
24	(*t*)	0.3673	0.3718	0.5174	0.573	0.4531	0.3569	0.269	0.0788	0
25	(*t*)	0.3722	0.3601	0.5057	0.5917	0.4718	0.3511	0.2632	0.073	0
121	(*g*)	0.37171	0.33410	0.48131	0.58849	0.46877	0.35459	0.26531	0.07535	0
122	(*g*)	0.37181	0.33337	0.48062	0.58875	0.46928	0.35495	0.26477	0.07463	0
26	(*u*)	0.3751	0.3487	0.4955	0.5738	0.4689	0.3586	0.2723	0.0857	0
27	(*v*)	0.3726	0.3433	0.484	0.5882	0.4648	0.3581	0.2693	0.0777	0
123	(*g*)	0.37184	0.33960	0.48233	0.58906	0.46581	0.35774	0.26679	0.07500	0
124	(*g*)	0.37156	0.33829	0.48167	0.58948	0.46668	0.35786	0.26605	0.07454	0
29	(*w*)	0.3685	0.3306	0.481	0.5827	0.4644	0.3441	0.2612	0.0788	0.25

Table 2 (continued)

Label No.	Ref.	*By*	O1*x*	O1*y*	O2*x*	O2*y*	O3*x*	O3*y*	O3*z*	*Xz*
125	(*g*)	0.36776	0.33069	0.48154	0.58491	0.46507	0.34423	0.25882	0.07756	0.25
126	(*g*)	0.36769	0.32873	0.48054	0.58422	0.46518	0.34398	0.25907	0.07719	0.25
127	(*g*)	0.36764	0.32850	0.48080	0.58495	0.46579	0.34394	0.25860	0.07669	0.25
30	(*w*)	0.3682	0.3159	0.4835	0.5962	0.4705	0.3405	0.2498	0.0671	0.25
128	(*g*)	0.36738	0.31489	0.48288	0.59891	0.47167	0.34048	0.24738	0.06546	0.25
129	(*g*)	0.36728	0.31390	0.48277	0.60000	0.47268	0.34044	0.24670	0.06482	0.25
31	(*x*)	0.367	0.3232	0.4841	0.5961	0.4655	0.3449	0.2509	0.0658	0.25
130	(*g*)	0.36612	0.32218	0.48470	0.59839	0.46744	0.34556	0.24835	0.06422	0.25
131	(*g*)	0.36567	0.32113	0.48431	0.59905	0.46806	0.34574	0.24745	0.06377	0.25
132	(*g*)	0.37227	0.33088	0.47706	0.57941	0.47027	0.34935	0.26776	0.08645	0
32	(*v*)	0.3712	0.3473	0.4802	0.5814	0.4601	0.3583	0.2724	0.0875	0
133	(*g*)	0.36943	0.34189	0.47696	0.58170	0.46173	0.35745	0.26849	0.08480	0
134	(*g*)	0.36952	0.34212	0.47754	0.58217	0.46199	0.35720	0.26826	0.08491	0
33	(*y*)	0.3718	0.3432	0.4806	0.579	0.4633	0.3568	0.271	0.0874	0
135	(*g*)	0.37130	0.33887	0.47798	0.58097	0.46463	0.35495	0.26890	0.08485	0
136	(*g*)	0.37040	0.33771	0.47648	0.58081	0.46450	0.35524	0.26834	0.08483	0
137	(*g*)	0.37051	0.33796	0.47702	0.58134	0.46513	0.35498	0.26804	0.08462	0
138	(*g*)	0.36732	0.32421	0.48025	0.59147	0.46693	0.34642	0.25423	0.07585	0.25
139	(*g*)	0.36730	0.32388	0.48057	0.59219	0.46773	0.34654	0.25375	0.07534	0.25
140	(*g*)	0.37262	0.31506	0.47633	0.59261	0.47675	0.34816	0.25832	0.07647	0
141	(*g*)	0.37398	0.31292	0.47620	0.59484	0.48060	0.34878	0.25802	0.07370	0
35	(*j*)	0.384	0.333	0.497	0.599	0.485	0.359	0.269	0.065	0
36	(*z*)	0.3787	0.3309	0.5005	0.6006	0.4604	0.3812	0.2873	0.0463	0
142	(*g*)	0.38092	0.33092	0.49646	0.60399	0.48352	0.35593	0.26449	0.06234	0
143	(*g*)	0.38113	0.32968	0.49581	0.60399	0.48427	0.35642	0.26448	0.06120	0

References: (*a*) Comodi *et al.* (2001); (*b*) Majid & Hussain (1996); (*c*) Saenger & Kuhs (1992); (*d*) de Boer *et al.* (1991); (*e*) Mackie & Young (1973); (*f*) Sudarsanan *et al.* (1972); (*g*) *ab initio* (this work); (*h*) Elliot *et al.* (1981); (*i*) Akao *et al.* (1989); (*j*) Dai & Hughes (1989); (*k*) Hashimoto & Matsumoto (1998); (*l*) Kim *et al.* (2000); (*m*) Belokoneva *et al.* (1982); (*n*) Sudarsanan *et al.* (1973); (*o*) Ivanov *et al.* (1976); (*p*) Dai *et al.* (1991); (*q*) Calos & Kennard (1990); (*r*) Rouse *et al.* (1984); (*s*) Sudarsanan & Young (1974); (*t*) Nötzold *et al.* (1994); (*u*) Nötzold & Wulff (1998); (*v*) Alberius-Henning, Mattsson & Lidin (2000); (*w*) Corker *et al.* (1995); (*x*) Carrillo-Cabrera & von Schnering (1999); (*y*) Hata *et al.* (1979); (*z*) Trotter & Barnes (1958).

(ii) $A^{\rm II}O_6X_{1,2}$ polyhedra with intrinsically irregular coordination located within the one-dimensional channels extending in the *c* direction that are formed by the $(A^{\rm I}O_6)$–(BO_4) polyhedral arrangement.

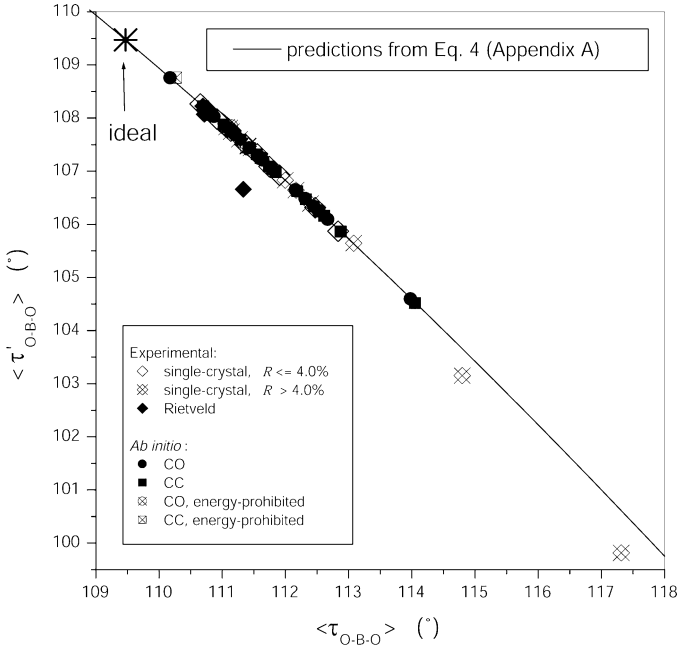

Figure 2
Average O—*B*—O bond angle $\langle\tau'_{\rm O-B-O}\rangle$ [see (1*b*)] as a function of $\langle\tau_{\rm O-B-O}\rangle$ [see (1*a*)].

In recent contributions (White *et al.*, 2005; Dong & White, 2004*a*,*b*; White & Dong, 2003), the geometrical aspects of the apatite structure were derived from regular (001) triangular anion nets. Deviations from this idealization proved useful in tracking the systematic crystallographic changes in the solid-solution series.

The stoichiometries of stable apatite-type compounds are intimately linked to the expression of their crystallographic and electronic structures. While it is expected that the structural and physical properties of a given apatite will depend mainly on its chemical composition, factors such as synthesis, equilibration times and cationic ordering over distinct crystallographic sites often induce modifications at the unit-cell scale (Dong & White, 2004*a*,*b*; Ferraris *et al.*, 2005). Developing a fundamental crystal-chemical understanding of the links between the equilibration conditions (total pressure, temperature, prevailing gas fugacities, ambient chemical potentials *etc.*), the crystallographic features and the chemical compositions of a range of apatites would enhance the directed design of apatite-type materials with tailored structural and crystal-chemical properties. A knowledge base of this depth would certainly be useful in emerging applications such as the treatment of lead-contaminated soils and waters (Chen *et al.*, 1997; Zhang & Ryan, 1999; Ioannidis & Zouboulis, 2003), the co-stabilization and recycling of incinerator ash with industrial and/or mining wastes (Eighmy *et al.*, 1998; Valsami-Jones *et al.*, 1998; Crannell *et al.*, 2000; Dong *et al.*, 2002; Dong & White, 2004*a*,*b*; Kim *et al.*, 2005) and the development of apatite-type oxygen-ion conductors for the electrolyte in solid oxygen fuel cells (Slater *et al.*, 2004).

The quality of apatite crystal structure refinements has been the subject of some discussion (Felsche, 1972; McConnell, 1973; White *et al.*, 2005). While single-crystal determinations are most reliable, doubts remain concerning the correlation of structure and chemistry. For example, in phosphate apatites differentiating the mode of $PO_4 \leftrightarrow CO_3$ replacement as *A* or *B* types is particularly difficult. In instances where there is cation mixing over the $A^{\rm I}$ and $A^{\rm II}$ sites, the partitioning coefficient is strongly dependent on the equilibration conditions. Even in gem-grade single crystals, micro-domains of distinctive composition have been recently shown to exist (Ferraris *et al.*, 2005). As a further complication, in the case of the *X* anion the possibility of incommensurate ordering cannot be ruled out (Alberius-Henning, Moustiakimov & Lidin, 2000; Christy *et al.*, 2001). Where powder methods are used, the possibility of an error increases.

Consequently, there is a need to develop analytical methods to check the validity of apatite refinements that go beyond the normal considerations of bond length, bond angle, *R* factor and so on. A preliminary approach was used by White & Dong (2003) to correlate the geometric parameters, specifically the $A^{\rm I}O_6$ metaprism twist angle to composition, and in the case of calcium–lead fluoro-vanadinites (Dong & White, 2004*a*,*b*) with the mode of synthesis. Geometric considerations can also be used to detect the apatite structures that are intrinsically flawed or erroneous due to unexpected departures in composition. For example, in the chemical series $Ca_{10-x}Pb_x(PO_4)_6Br_2$ that was studied by powder neutron diffraction, the metaprism twist was used to identify materials in thermodynamic disequilibrium and the loss of bromine (Kim, 2001; White *et al.*, 2005).

In the present paper, a geometric crystal-chemical model of $P6_3/m$ apatite with cell content $(A^{\rm I}{}_4)(A^{\rm II}{}_6)(BO_4)_6X_2$ is developed following a geometrical parameterization based on algebraically independent parameters representing the distortions of the $A^{\rm I}O_6$, BO_4 and $A^{\rm II}O_6X_{1,2}$ polyhedra. The model summarizes the main polyhedral distortions observed in apatite-type materials *via* convenient crystal-chemical parameters. It also provides a way to control the least-squares minimization process in a structure refinement using physical parameters (*i.e.* bond lengths and angles). Here, previously published lattice parameters and structural refinement data for 18 end-member compositions are compared with the optimized atomic coordinates and cell parameters computed by *ab initio* total-energy minimization simulations. When analyzed in light of the geometric crystal-chemical model, these results reveal that $\ldots$–$A^{\rm II}$–O3–*B*–O3–$A^{\rm II}$–$\cdots$ chains located in the one-dimensional channels of apatite control the magnitude of the *c* lattice parameter, whereas that of *a* is determined by the $(A^{\rm I}O_6)$–(BO_4) polyhedral arrangement.

2. Materials and methods

2.1. Geometrical parameterization of $P6_3/m$ apatite

Assuming cation-centered $A^{\rm I}O_6$ polyhedra and BO_4 tetrahedra with uniform O—*B*—O bond-angle bending, and four equal B—O bond lengths, one can show (*Appendix A*) that the crystallographic description of $P6_3/m$ apatite (*a*, *c*, 12 atom coordinates = 14 crystallographic parameters) is equivalent to a geometrical parameterization based on the following crystal-chemical parameters (Fig. 1): $A^{\rm I}$—O1 bond length, $d_{A^{\rm I}-{\rm O1}}$; difference between $A^{\rm I}$—O1 and $A^{\rm I}$—O2 bond lengths, $\Delta_{A^{\rm I}-{\rm O}}$; angle that an $A^{\rm I}$—O1 bond makes with respect to *c*, $\psi_{A^{\rm I}-{\rm O1}}$; counter-rotation angle of $A^{\rm I}O_6$ polyhedra, $\delta_{A^{\rm I}}$; orientation of $A^{\rm I}O_6$ polyhedra with respect to *a*, $\alpha_{A^{\rm I}}$; BO_4 bond length, $d_{B-{\rm O}}$; O—*B*—O bond-bending angle, $\tau_{{\rm O}-B-{\rm O}}$; $A^{\rm II}$—$A^{\rm II}$ triangular side length, $\rho_{A^{\rm II}}$ or $A^{\rm II}$—*X* bond length, $d_{A^{\rm II}-X}$; orientation of $A^{\rm II}$—$A^{\rm II}$—$A^{\rm II}$ triangles with respect to *a*, $\alpha_{A^{\rm II}}$; $A^{\rm II}$—O3 bond length, $d_{A^{\rm II}-{\rm O3}}$; and O3—$A^{\rm II}$—O3 bond angle, $\phi_{{\rm O3}-A^{\rm II}-{\rm O3}}$.

This geometrical parameterization allows the prediction of all atomic positions in an (idealized) apatite structure using ten algebraically independent crystal-chemical parameters ($d_{A^{\rm I}-{\rm O1}}$, $\Delta_{A^{\rm I}-{\rm O}}$, $\delta_{A^{\rm I}}$, $\alpha_{A^{\rm I}}$, $d_{B-{\rm O}}$, $\tau_{{\rm O}-B-{\rm O}}$, $\rho_{A^{\rm II}}$ or $d_{A^{\rm II}-X}$, $d_{A^{\rm II}-{\rm O3}}$, $\phi_{{\rm O3}-A^{\rm II}-{\rm O3}}$ and $\alpha_{A^{\rm II}}$; Fig. 1). By contrast, 14 crystallographic parameters (Table 1) are used in a structure refinement in the space group $P6_3/m$ (12 atomic coordinates and two unit-cell parameters). The difference in the number of independent parameters (14 for the crystallographic description *versus* 10 for the geometrical parameterization) is due to four geometric constraints [$A^{\rm I}z = 0$; see equations (19), (20) and (21); see *Appendix A*], three of them arising from the assumption of uniform bond-angle bending of BO_4 tetrahedra with four equal *B*—O bond lengths, and the fourth from constraining to zero the *z* coordinate of $A^{\rm I}$ cations so as to have cation-centered $A^{\rm I}O_6$ polyhedra.

Table 1(*a*) summarizes a first set of equations to produce a crystallographic description of $P6_3/m$ apatite from the crystal-chemical parameters, *i.e.* gives the cell parameters and the fractional atomic coordinates for each atom in the asymmetric unit as functions of the ten algebraically independent crystal-chemical degrees of freedom that are assumed. Table 1(*b*) summarizes a second set of equations for the converse problem of the decomposition of the crystallographic description of $P6_3/m$ apatite into its crystal-chemical parameters. The two sets of equations are not entirely equivalent because of the reduction in the number of independent parameters.

A given set of cell parameters and atomic coordinates then produces an equivalent set of crystal-chemical parameters through a second set of equations (Table 1*b*). Processing these crystal-chemical parameters through equations of the first set (Table 1*a*) produces unit-cell parameters and fractional atomic coordinates that are marginally different from the initial ones because the structure has been regularized by geometric constraints. Although this initial transformation results in slight differences from the original structure, further transformations between the crystallographic description and the geometrical parameterization based on the equations in Tables 1(*a*) and (*b*) are fully reversible within numerical accuracy.

Table 3
Crystal-chemical parameters extracted from the crystallographic descriptions (*a*, *c*, atomic coordinates; Table 2) using the equations given in Table 1(*b*), for both experimental and *ab initio* optimized structures.

(*a*)

Label No.	Composition	Type	R (%)	E_{total} (eV per unit cell)	$(A^{I}-O1)$ (Å)	$(A^{I}-O1)^{A^{I}z=0}$ (Å)	$\Delta_{A^{I}-O}$ (Å)	$\Delta_{A^{I}-O}^{A^{I}z=0}$ (Å)	$\psi_{A^{I}-O1}$ (°)	$\psi_{A^{I}-O1}^{A^{I}z=0}$ (°)	$\delta_{A^{I}}$ (°)
1	$Ca_{10}(PO_4)_6F_2$	Single *Xtal*	2.50		2.3991	2.4045	0.0574	0.0467	44.398	44.272	18.244
2	$Ca_{10}(PO_4)_6F_2$	Rietveld	–	–	2.3796	2.3885	0.0748	0.0572	44.133	43.926	18.363
3	$Ca_{10}(PO_4)_6F_2$	Single *Xtal*	2.50	–	2.4008	2.4063	0.0551	0.0442	44.481	44.353	18.300
4	$Ca_{10}(PO_4)_6F_2$	Single *Xtal*	2.30	–	2.3981	2.4033	0.0556	0.0452	44.358	44.236	18.236
5	$Ca_{10}(PO_4)_6F_2$	Single *Xtal*	4.40	–	2.3861	2.3925	0.0631	0.0504	44.152	44.003	18.374
6	$Ca_{10}(PO_4)_6F_2$	Single *Xtal*	1.60	–	2.3966	2.4021	0.0559	0.0451	44.363	44.237	18.252
7	$Ca_{10}(PO_4)_6F_2$	Single *Xtal*	2.90	–	2.3919	2.3978	0.0590	0.0473	44.322	44.184	18.343
8	$Ca_{10}(PO_4)_6F_2$	Single *Xtal*	1.60	–	2.3967	2.4021	0.0559	0.0451	44.364	44.238	18.252
101	$Ca_{10}(PO_4)_6F_2$	CO	–	−303.035	2.3940	2.3986	0.0554	0.0462	44.258	44.151	18.236
102	$Ca_{10}(PO_4)_6F_2$	CO	–	−303.052	2.3955	2.4002	0.0554	0.0459	44.277	44.166	18.247
103	$Ca_{10}(PO_4)_6F_2$	CC	–	−303.113	2.3768	2.3787	0.0558	0.0520	43.984	43.940	18.348
9	$Ca_{10}(PO_4)_6Br_2$	Single *Xtal*	3.08	–	2.4153	2.4362	0.0231	−0.0190	46.767	46.247	22.583
104	$Ca_{10}(PO_4)_6Br_2$	CO	–	−296.112	2.4050	2.4255	0.0247	−0.0165	46.513	46.005	22.760
105	$Ca_{10}(PO_4)_6Br_2$	CC	–	−296.153	2.3928	2.4133	0.0271	−0.0143	46.599	46.086	22.705
10	$Pb_{10}(PO_4)_6Cl_2$	Single *Xtal*	5.20	–	2.5507	2.5772	0.1366	0.0841	45.160	44.570	20.465
11	$Pb_{10}(PO_4)_6Cl_2$	Single *Xtal*	2.10	–	2.5563	2.5813	0.1217	0.0722	45.161	44.606	21.197
12	$Pb_{10}(PO_4)_6Cl_2$	Single *Xtal*	5.80	–	2.5483	2.5748	0.1365	0.0841	45.185	44.594	20.465
106	$Pb_{10}(PO_4)_6Cl_2$	CO	–	−270.056	2.6286	2.6104	0.0024	0.0385	44.904	45.304	20.320
107	$Pb_{10}(PO_4)_6Cl_2$	CC	–	−270.046	2.5765	2.5942	0.0861	0.0509	45.739	45.339	19.977
108	$Pb_{10}(PO_4)_6Br_2$	CO	–	−268.573	2.6094	2.6317	0.0426	−0.0024	46.151	45.646	20.830
109	$Pb_{10}(PO_4)_6Br_2$	CC	–	−268.597	2.6039	2.6251	0.0387	−0.0037	46.382	45.901	20.679
16	$Pb_{10}(PO_4)_6F_2$	Single *Xtal*	4.90	–	2.4823	2.4978	0.2640	0.2344	43.393	43.059	18.229
110	$Pb_{10}(PO_4)_6F_2$	CO	–	−272.892	2.5432	2.5513	0.0597	0.0437	44.508	44.330	18.855
111	$Pb_{10}(PO_4)_6F_2$	CC	–	−272.952	2.5581	2.5663	0.0571	0.0407	44.530	44.349	18.789
112	$Pb_{10}(PO_4)_6F_2$	CO	–	−272.902	2.5523	2.5596	0.0433	0.0288	44.682	44.521	19.118
17	$Cd_{10}(PO_4)_6Cl_2$	Single *Xtal*	5.60	–	2.3089	2.3331	0.0678	0.0193	46.614	45.989	21.666
18	$Cd_{10}(PO_4)_6Cl_2$	Single *Xtal*	7.50	–	2.2995	2.3195	0.0841	0.0443	46.001	45.492	20.654
113	$Cd_{10}(PO_4)_6Cl_2$	CO	–	−234.875	2.2221	2.2218	0.1131	0.1136	43.142	43.149	28.010
114	$Cd_{10}(PO_4)_6Cl_2$	CC	–	−234.289	2.3194	2.2446	0.0053	0.1482	41.624	43.344	27.417
115	$Cd_{10}(PO_4)_6Cl_2$	CO	–	−236.162	2.3205	2.3345	0.0706	0.0427	46.211	45.853	20.894
116	$Cd_{10}(PO_4)_6Cl_2$	CC	–	−236.221	2.3150	2.3287	0.0667	0.0396	46.613	46.260	21.531
19	$Pb_{10}(AsO_4)_6Cl_2$	Single *Xtal*	2.70	–	2.4835	2.5214	0.2753	0.2017	43.458	42.646	19.453
20	$Pb_{10}(AsO_4)_6Cl_2$	Single *Xtal*	3.10	–	2.4960	2.5337	0.2375	0.1638	43.760	42.948	21.001
21	$Pb_{10}(AsO_4)_6Cl_2$	Single *Xtal*	5.70	–	2.5221	2.5572	0.2604	0.1923	43.973	43.219	20.623
117	$Pb_{10}(AsO_4)_6Cl_2$	CO	–	−243.189	2.5341	2.5533	0.1862	0.1487	43.831	43.418	20.174
118	$Pb_{10}(AsO_4)_6Cl_2$	CC	–	−243.192	2.5228	2.5429	0.1996	0.1603	43.974	43.538	20.427
22	$Ca_4Pb_6(AsO_4)_6Cl_2$	Single *Xtal*	6.20	–	2.3812	2.4287	0.1671	0.0729	43.350	42.302	27.338
119	$Ca_4Pb_6(AsO_4)_6Cl_2$	CO	–	−254.488	2.4088	2.4392	0.1022	0.0416	43.240	42.572	26.939
120	$Ca_4Pb_6(AsO_4)_6Cl_2$	CC	–	−254.514	2.4007	2.4305	0.1008	0.0414	43.564	42.900	26.980
23	$Sr_{10}(PO_4)_6Cl_2$	Single *Xtal*	3.40	–	2.5673	2.5718	0.0127	0.0036	45.638	45.535	19.448
24	$Sr_{10}(PO_4)_6Cl_2$	Rietveld	–	–	2.4658	2.4715	0.1049	0.0936	43.475	43.349	22.611
25	$Sr_{10}(PO_4)_6Cl_2$	Rietveld	–	–	2.4997	2.4997	0.0814	0.0814	44.028	44.028	23.660
121	$Sr_{10}(PO_4)_6Cl_2$	CO	–	−295.014	2.5644	2.5688	0.0191	0.0103	45.569	45.469	19.501
122	$Sr_{10}(PO_4)_6Cl_2$	CC	–	−295.037	2.5570	2.5615	0.0190	0.0099	45.718	45.614	19.456
26	$Sr_{10}(PO_4)_6Br_2$	Rietveld	–	–	2.5489	2.5377	0.1194	0.1414	44.514	44.765	20.208
27	$Sr_{10}(PO_4)_6Br_2$	Single *Xtal*	5.20	–	2.5922	2.6003	−0.0130	−0.0294	46.274	46.086	20.463
123	$Sr_{10}(PO_4)_6Br_2$	CO	–	−293.271	2.5907	2.5982	−0.0103	−0.0254	46.213	46.041	20.116
124	$Sr_{10}(PO_4)_6Br_2$	CC	–	−293.306	2.5788	2.5868	−0.0057	−0.0217	46.212	46.028	20.033
29	$(Sr_{0.992}Nd_{0.005})_{10}(PO_4)_6F_2$	Single *Xtal*	2.30	–	2.5545	2.5534	0.0212	0.0232	44.509	44.532	18.236
125	$Sr_{10}(PO_4)_6F_2$	CO	–	−299.539	2.5550	2.5517	0.0122	0.0188	44.362	44.435	18.492
126	$Sr_{10}(PO_4)_6F_2$	CO	–	−299.509	2.5516	2.5504	0.0205	0.0230	44.434	44.461	18.169
127	$Sr_{10}(PO_4)_6F_2$	CC	–	−299.547	2.5380	2.5367	0.0226	0.0252	44.369	44.398	18.240
30	$(Sr_{0.982}Nd_{0.012})_{10}(VO_4)_6F_2$	Single *Xtal*	2.20	–	2.5522	2.5544	0.0583	0.0540	43.361	43.316	17.780
128	$Sr_{10}(VO_4)_6F_2$	CO	–	−319.161	2.5521	2.5557	0.0532	0.0461	43.422	43.346	17.979
129	$Sr_{10}(VO_4)_6F_2$	CC	–	−319.229	2.5354	2.5394	0.0569	0.0488	43.328	43.241	17.997
31	$Sr_{10}(VO_4)_6CuO$	Single *Xtal*	6.70	–	2.5756	2.5836	0.0197	0.0038	44.323	44.150	18.560
130	$Sr_{10}(VO_4)_6CuO$	CO	–	−327.534	2.5845	2.5761	−0.0050	0.0118	43.798	43.978	18.751
131	$Sr_{10}(VO_4)_6CuO$	CC	–	−327.582	2.5718	2.5631	−0.0045	0.0130	43.728	43.915	18.705
132	$Ba_{10}(PO_4)_6F_2$	CO	–	−299.866	2.7267	2.7196	0.0389	0.0530	44.547	44.695	18.322
32	$Ba_{10}(PO_4)_6Br_2$	Single *Xtal*	3.28	–	2.7680	2.7745	−0.0535	−0.0667	46.402	46.261	20.012
133	$Ba_{10}(PO_4)_6Br_2$	CO	–	−294.796	2.7689	2.7767	−0.0439	−0.0598	46.474	46.304	19.446
134	$Ba_{10}(PO_4)_6Br_2$	CC	–	−294.800	2.7616	2.7696	−0.0409	−0.0571	46.331	46.157	19.536
33	$Ba_{10}(PO_4)_6Cl_2$	Single *Xtal*	3.40	–	2.7394	2.7431	−0.0038	−0.0113	45.870	45.790	19.482
135	$Ba_{10}(PO_4)_6Cl_2$	CO	–	−296.501	2.7425	2.7455	−0.0104	−0.0163	45.901	45.837	19.176
136	$Ba_{10}(PO_4)_6Cl_2$	CO	–	−296.503	2.7506	2.7521	−0.0198	−0.0228	46.004	45.972	19.001
137	$Ba_{10}(PO_4)_6Cl_2$	CC	–	−296.513	2.7394	2.7434	−0.0106	−0.0186	45.954	45.867	19.120

Table 3 (continued)

Label No.	Composition	Type	R (%)	E_{total} (eV per unit cell)	$(A^{I}-O1)$ (Å)	$(A^{I}-O1)^{A^{I}z=0}$ (Å)	$\Delta_{A^{I}-O}$ (Å)	$\Delta_{A^{I}-O}^{A^{I}z=0}$ (Å)	$\psi_{A^{I}-O1}$ (°)	$\psi_{A^{I}-O1}^{A^{I}z=0}$ (°)	$\delta_{A^{I}}$ (°)
138	$Ba_{10}(MnO_4)_6F_2$	CO	–	−295.790	2.7297	2.7221	−0.0069	0.0081	43.611	43.762	18.343
139	$Ba_{10}(MnO_4)_6F_2$	CC	–	−295.830	2.7141	2.7070	−0.0013	0.0128	43.538	43.681	18.411
140	$Ba_{10}(MnO_4)_6F_2$	CO		−295.136	2.7369	2.7212	0.0386	0.0697	43.425	43.741	17.721
141	$Ba_{10}(MnO_4)_6F_2$	CC	–	−295.516	2.6878	2.6718	0.0575	0.0890	43.572	43.900	17.822
35	$Pb_{10}(VO_4)_6Cl_2$	Single *Xtal*	2.20	–	2.4939	2.5345	0.2637	0.1847	44.526	43.631	21.185
36	$Pb_{10}(VO_4)_6Cl_2$	Single *Xtal*	11.50	–	2.4760	2.5049	0.0935	0.0358	43.497	42.872	19.801
142	$Pb_{10}(VO_4)_6Cl_2$	CO	–	−291.537	2.4953	2.5310	0.2195	0.1498	44.331	43.548	21.322
143	$Pb_{10}(VO_4)_6Cl_2$	CC	–	−291.564	2.4882	2.5199	0.2170	0.1551	44.426	43.724	21.173

(*b*)

Label No.	Composition	Type	$\varphi_{A^{I}}$ (°)	$\alpha_{A^{I}}$ (°)	$\langle B-O\rangle$ (Å)	$\langle\tau_{O-B-O}\rangle$ (°)	$\rho_{A^{II}}$ (Å)	$(A^{II}-X)$ (Å)	$\alpha_{A^{II}}$ (°)	$(A^{II}-O3)$ (Å)	$\phi_{O3-A^{II}-O3}$ (°)
1	$Ca_{10}(PO_4)_6F_2$	Single *Xtal*	23.512	−20.082	1.5335	111.033	3.9819	2.2990	118.541	2.3502	139.828
2	$Ca_{10}(PO_4)_6F_2$	Rietveld	23.273	−20.280	1.5499	110.773	3.9830	2.2996	118.585	2.3276	139.748
3	$Ca_{10}(PO_4)_6F_2$	Single *Xtal*	23.399	−20.072	1.5348	110.994	3.9935	2.3056	118.561	2.3492	140.014
4	$Ca_{10}(PO_4)_6F_2$	Single *Xtal*	23.528	−20.190	1.5357	111.056	3.9798	2.2978	118.563	2.3511	140.115
5	$Ca_{10}(PO_4)_6F_2$	Single *Xtal*	23.253	−20.313	1.5392	111.145	3.9836	2.2999	118.504	2.3494	139.793
6	$Ca_{10}(PO_4)_6F_2$	Single *Xtal*	23.496	−20.231	1.5357	111.134	3.9784	2.2969	118.563	2.3491	139.741
7	$Ca_{10}(PO_4)_6F_2$	Single *Xtal*	23.314	−20.159	1.5353	111.111	3.9753	2.2951	118.563	2.3470	139.754
8	$Ca_{10}(PO_4)_6F_2$	Single *Xtal*	23.496	−20.231	1.5358	111.134	3.9786	2.2970	118.563	2.3491	139.740
101	$Ca_{10}(PO_4)_6F_2$	CO	23.529	−20.708	1.5522	111.149	3.9668	2.2902	118.776	2.3429	139.005
102	$Ca_{10}(PO_4)_6F_2$	CO	23.505	−20.669	1.5526	111.156	3.9705	2.2924	118.820	2.3447	138.953
103	$Ca_{10}(PO_4)_6F_2$	CC	23.304	−20.982	1.5506	111.129	3.9317	2.2699	118.454	2.3239	139.304
9	$Ca_{10}(PO_4)_6Br_2$	Single *Xtal*	14.835	−17.079	1.5371	111.908	4.4187	3.0572	122.298	2.3443	130.728
104	$Ca_{10}(PO_4)_6Br_2$	CO	14.479	−17.361	1.5560	112.160	4.3955	3.0461	123.019	2.3480	128.648
105	$Ca_{10}(PO_4)_6Br_2$	CC	14.591	−17.584	1.5540	112.185	4.3685	3.0271	122.842	2.3296	128.370
10	$Pb_{10}(PO_4)_6Cl_2$	Single *Xtal*	19.069	−18.582	1.5354	111.402	4.3597	3.1155	121.183	2.6634	134.789
11	$Pb_{10}(PO_4)_6Cl_2$	Single *Xtal*	17.606	−18.556	1.5376	111.076	4.3485	3.1113	121.057	2.6565	135.112
12	$Pb_{10}(PO_4)_6Cl_2$	Single *Xtal*	19.069	−18.582	1.5342	111.411	4.3574	3.1130	121.183	2.6601	134.755
106	$Pb_{10}(PO_4)_6Cl_2$	CO	19.360	−19.239	1.5617	111.645	4.3200	3.0971	120.879	2.6297	133.370
107	$Pb_{10}(PO_4)_6Cl_2$	CC	20.046	−19.511	1.5597	111.609	4.2952	3.0781	120.723	2.6045	133.287
108	$Pb_{10}(PO_4)_6Br_2$	CO	18.340	−18.399	1.5622	111.785	4.4513	3.1606	121.154	2.6321	133.722
109	$Pb_{10}(PO_4)_6Br_2$	CC	18.641	−18.531	1.5606	111.847	4.4473	3.1512	120.826	2.6069	133.620
16	$Pb_{10}(PO_4)_6F_2$	Single *Xtal*	23.543	−21.164	1.5660	111.071	4.0387	2.3318	120.540	2.5812	136.142
110	$Pb_{10}(PO_4)_6F_2$	CO	22.291	−18.994	1.5563	111.138	4.1867	2.4172	118.305	2.5434	141.440
111	$Pb_{10}(PO_4)_6F_2$	CC	22.421	−18.846	1.5579	111.023	4.2078	2.4294	118.636	2.5645	141.222
112	$Pb_{10}(PO_4)_6F_2$	CO	21.763	−19.030	1.5553	111.075	4.1869	2.4173	118.224	2.5466	140.695
17	$Cd_{10}(PO_4)_6Cl_2$	Single *Xtal*	16.668	−16.570	1.5413	111.998	4.3932	2.5364	123.545	2.2021	131.620
18	$Cd_{10}(PO_4)_6Cl_2$	Single *Xtal*	18.691	−16.937	1.5497	113.081	4.3517	2.5125	122.681	2.2271	132.232
113	$Cd_{10}(PO_4)_6Cl_2$	CO	3.979	−8.920	1.5499	111.145	4.3481	2.5104	123.559	2.1341	145.035
114	$Cd_{10}(PO_4)_6Cl_2$	CC	5.166	−8.740	1.5507	110.268	4.5167	2.6077	123.351	2.1269	149.339
115	$Cd_{10}(PO_4)_6Cl_2$	CO	18.212	−18.317	1.5559	112.521	4.1810	2.9105	123.298	2.2387	127.899
116	$Cd_{10}(PO_4)_6Cl_2$	CC	16.937	−17.760	1.5561	112.613	4.1915	2.9066	124.207	2.2316	125.202
19	$Pb_{10}(AsO_4)_6Cl_2$	Single *Xtal*	21.093	−22.817	1.6827	112.833	4.4003	3.1454	120.897	2.6347	132.443
20	$Pb_{10}(AsO_4)_6Cl_2$	Single *Xtal*	17.999	−22.566	1.6901	111.552	4.4000	3.1453	120.937	2.5751	131.910
21	$Pb_{10}(AsO_4)_6Cl_2$	Single *Xtal*	18.755	−21.881	1.6703	112.398	4.4264	3.1629	120.836	2.6346	132.323
117	$Pb_{10}(AsO_4)_6Cl_2$	CO	19.653	−22.670	1.7203	112.671	4.3334	3.1143	121.239	2.5848	129.476
118	$Pb_{10}(AsO_4)_6Cl_2$	CC	19.146	−22.442	1.7202	112.876	4.3475	3.1142	121.733	2.5803	128.097
22	$Ca_4Pb_6(AsO_4)_6Cl_2$	Single *Xtal*	5.324	−17.856	1.7053	117.314	4.4136	3.1177	122.805	2.5378	126.209
119	$Ca_4Pb_6(AsO_4)_6Cl_2$	CO	6.123	−18.268	1.7190	113.979	4.3433	3.0846	123.536	2.5198	123.580
120	$Ca_4Pb_6(AsO_4)_6Cl_2$	CC	6.040	−18.277	1.7185	114.049	4.3405	3.0740	123.653	2.4993	122.486
23	$Sr_{10}(PO_4)_6Cl_2$	Single *Xtal*	21.103	−18.604	1.5397	111.368	4.3401	3.0861	117.969	2.5097	139.541
24	$Sr_{10}(PO_4)_6Cl_2$	Rietveld	14.778	−11.428	1.5254	111.333	4.3384	3.0829	118.102	2.5259	138.717
25	$Sr_{10}(PO_4)_6Cl_2$	Rietveld	12.680	−16.087	1.5851	110.718	4.3204	3.0745	118.565	2.4818	138.664
121	$Sr_{10}(PO_4)_6Cl_2$	CO	20.999	−19.296	1.5562	111.202	4.3032	3.0689	118.090	2.5073	138.482
122	$Sr_{10}(PO_4)_6Cl_2$	CC	21.089	−19.447	1.5552	111.290	4.2814	3.0529	118.129	2.4940	137.777
26	$Sr_{10}(PO_4)_6Br_2$	Rietveld	19.585	−15.952	1.4936	110.693	4.4621	3.1437	117.754	2.5674	140.900
27	$Sr_{10}(PO_4)_6Br_2$	Single *Xtal*	19.073	−17.830	1.5386	111.273	4.4907	3.1583	118.324	2.5207	139.381
123	$Sr_{10}(PO_4)_6Br_2$	CO	19.768	−18.458	1.5582	111.431	4.4695	3.1483	118.595	2.5107	138.071
124	$Sr_{10}(PO_4)_6Br_2$	CC	19.933	−18.722	1.5566	111.435	4.4378	3.1289	118.336	2.4968	138.067
29	$(Sr_{0.992}Nd_{0.005})_{10}(PO_4)_6F_2$	Single *Xtal*	23.528	−18.972	1.5404	110.652	4.1505	2.3963	117.092	2.5224	143.283
125	$Sr_{10}(PO_4)_6F_2$	CO	23.016	−19.205	1.5561	110.715	4.1616	2.4027	117.054	2.5170	143.056
126	$Sr_{10}(PO_4)_6F_2$	CO	23.662	−19.412	1.5560	110.719	4.1599	2.4017	117.148	2.5122	142.991
127	$Sr_{10}(PO_4)_6F_2$	CC	23.520	−19.548	1.5543	110.697	4.1378	2.3890	116.933	2.4967	143.119
30	$(Sr_{0.982}Nd_{0.012})_{10}(VO_4)_6F_2$	Single *Xtal*	24.439	−22.727	1.7110	111.742	4.2349	2.4450	117.847	2.5099	139.842
128	$Sr_{10}(VO_4)_6F_2$	CO	24.042	−23.206	1.7285	111.789	4.2326	2.4437	118.006	2.5041	138.961
129	$Sr_{10}(VO_4)_6F_2$	CC	24.006	−23.516	1.7259	111.739	4.1982	2.4238	117.730	2.4858	139.157

Table 3 (continued)

Label No.	Composition	Type	$\varphi_{A^{\rm I}}$ (°)	$\alpha_{A^{\rm I}}$ (°)	$\langle B-{\rm O}\rangle$ (Å)	$\langle\tau_{{\rm O}-B-{\rm O}}\rangle$ (°)	$\rho_{A^{\rm II}}$ (Å)	$(A^{\rm II}-X)$ (Å)	$\alpha_{A^{\rm II}}$ (°)	$(A^{\rm II}-{\rm O3})$ (Å)	$\phi_{{\rm O3}-A^{\rm II}-{\rm O3}}$ (°)
31	$Sr_{10}(VO_4)_6CuO$	Single *Xtal*	22.880	−21.390	1.7099	112.166	4.4691	2.5802	118.146	2.4947	139.648
130	$Sr_{10}(VO_4)_6CuO$	CO	22.499	−21.885	1.7297	112.314	4.4800	2.5865	118.216	2.4905	138.635
131	$Sr_{10}(VO_4)_6CuO$	CC	22.591	−22.135	1.7271	112.328	4.4516	2.5701	117.922	2.4755	138.818
132	$Ba_{10}(PO_4)_6F_2$	CO	23.356	−18.968	1.5614	110.177	4.1578	3.0822	116.467	2.7634	140.612
32	$Ba_{10}(PO_4)_6Br_2$	Single *Xtal*	19.975	−16.435	1.5378	110.753	4.6583	3.3035	116.969	2.7260	143.607
133	$Ba_{10}(PO_4)_6Br_2$	CO	21.108	−17.257	1.5603	110.870	4.6272	3.2889	116.894	2.7108	142.761
134	$Ba_{10}(PO_4)_6Br_2$	CC	20.927	−17.284	1.5597	110.844	4.6104	3.2811	116.722	2.7093	143.101
33	$Ba_{10}(PO_4)_6Cl_2$	Single *Xtal*	21.036	−16.921	1.5390	110.915	4.5086	3.2302	116.921	2.7293	142.108
135	$Ba_{10}(PO_4)_6Cl_2$	CO	21.647	−17.742	1.5594	110.849	4.4846	3.2191	116.904	2.7099	141.961
136	$Ba_{10}(PO_4)_6Cl_2$	CO	21.998	−17.871	1.5593	110.756	4.4772	3.2157	116.987	2.7131	141.552
137	$Ba_{10}(PO_4)_6Cl_2$	CC	21.759	−17.924	1.5591	110.705	4.4561	3.2044	116.801	2.7064	141.739
138	$Ba_{10}(MnO_4)_6F_2$	CO	23.314	−20.831	1.7059	111.573	4.4450	2.5663	116.490	2.7038	142.791
139	$Ba_{10}(MnO_4)_6F_2$	CC	23.179	−20.994	1.7045	111.545	4.4201	2.5520	116.319	2.6884	142.765
140	$Ba_{10}(MnO_4)_6F_2$	CO	24.559	−22.713	1.7082	111.431	4.1926	3.1184	117.426	2.7554	137.423
141	$Ba_{10}(MnO_4)_6F_2$	CC	24.356	−23.422	1.7033	111.379	4.0742	3.0396	117.046	2.6923	135.597
35	$Pb_{10}(VO_4)_6Cl_2$	Single *Xtal*	17.629	−21.283	1.7015	112.471	4.4500	3.1569	122.410	2.5743	127.757
36	$Pb_{10}(VO_4)_6Cl_2$	Single *Xtal*	20.397	−20.533	1.7422	114.796	4.4846	3.1739	122.119	2.5217	119.263
142	$Pb_{10}(VO_4)_6Cl_2$	CO	17.356	−22.031	1.7345	112.454	4.4102	3.1382	122.960	2.5661	126.535
143	$Pb_{10}(VO_4)_6Cl_2$	CC	17.655	−22.244	1.7333	112.539	4.3943	3.1230	122.781	2.5436	126.049

2.2. Treatment of published structural refinement data

The equations resulting from geometrical parameterization (Table 1) were used to analyze the crystallographic parameters for 18 chemical end-member $P6_3/m$ apatites selected from the literature (Table 2). To allow direct comparison with *ab initio* calculations, only the known fully ordered structures were considered. All experimental data used in this paper were obtained from the unit-cell parameters and atomic coordinates reported by the authors of the original articles. Depending on the type and quality of the crystal-structure determinations, the structure refinements were categorized into three groups (Table 2):

(i) single-crystal refinements with agreement factors $R \leq 4.0\%$,

(ii) single-crystal refinements with $R > 4.0\%$ and

(iii) Rietveld refinements from powder diffraction data.

The crystal-chemical parameters (Table 3) were extracted from the crystallographic parameters of experimental and *ab initio* optimized structures using the equations given in Table 1(*b*).

2.3. *Ab initio* modeling

The modeling and *ab initio* interface software environment *Materials Toolkit* (Le Page *et al.*, 2002; Le Page & Rodgers, 2005) was used to prepare the input files for *ab initio* total-energy minimization calculations with *VASP* (Kresse, 1993; Kresse & Hafner, 1993, 1994). The following execution parameters were used: GGA PAW potentials (Kresse & Joubert, 1999), electronic convergence at 1×10^{-7} eV, convergence for forces of 1×10^{-4} eV Å^{-1}, Davidson-blocked iterative optimization of the wavefunctions in combination with reciprocal-space projectors (Davidson, 1983), a $2 \times 2 \times 2$ k-mesh for the reciprocal space integration with a Monkhorst–Pack scheme (Monkhorst & Pack, 1976), and a Methfessel–Paxton smearing scheme of the order 1 and width 0.2 eV for energy corrections (Methfessel & Paxton, 1989). Spin polarization corrections were not used.

Coordinate-only (CO) optimizations using experimental lattice parameters and cell-and-coordinate (CC) optimizations were performed for the 18 end-member compositions (Table 2). Calculations took about 20 h per structure on a single 3 GHz Athlon-64 PC running serial VASP.4.6.3 under Microsoft® Windows® *XP*, using the execution scheme described above. The resulting *ab initio* coordinates and cell parameters are summarized in Table 2, along with the lattice parameters and fractional atomic coordinates obtained from published experimental (*i.e.* single-crystal or Rietveld) structure refinements.

3. Results and discussion

The reduction of independent parameters from 14 to 10 between the crystallographic description and the geometrical parameterization is due to four geometric constraints. We should then first examine the validity of the constraints assumed in the geometrical parameterization.

3.1. Comparison of the constraints with experimental and *ab initio* results

3.1.1. Bond-angle bending of BO_4 tetrahedra. Fig. 2 displays the average tetrahedral O—B—O bond angles $\langle\tau'_{{\rm O}-B-{\rm O}}\rangle$ as a function of $\langle\tau_{{\rm O}-B-{\rm O}}\rangle$ (Fig. 1*b*), where

$$\langle\tau_{{\rm O}-B-{\rm O}}\rangle = 1/3\cdot[\tau({\rm O1}-B-{\rm O2}) + 2\cdot\tau({\rm O1}-B-{\rm O3})] \qquad (1a)$$

$$\langle\tau'_{{\rm O}-B-{\rm O}}\rangle = 1/3\cdot\tau({\rm O2}-B-{\rm O3}) + 2\cdot\tau({\rm O3}-B-{\rm O3}')]. \qquad (1b)$$

The solid line shown represents the predictions made from (4) (see *Appendix A*). On the plot of the average BO_4 bond-angle values ($\langle\tau_{{\rm O}-B-{\rm O}}\rangle$, $\langle\tau'_{{\rm O}-B-{\rm O}}\rangle$), agreement within expected

experimental error is observed between the geometric crystal-chemical model predictions and the observations for both *ab initio* and experimental data, despite local distortions (*i.e.* the individual bond lengths, edge lengths and bond angles) actually occurring in the BO_4 tetrahedra. The only three notable exceptions correspond to two single-crystal determinations with $R > 4.0\%$ and one Rietveld refinement.

This relationship (Fig. 2) implies a local $3m$ pseudo-symmetry with a B—O1 axis for the BO_4 tetrahedra that is not imposed by the $P6_3/m$ space-group symmetry. This point, which has not previously been recognized, is supported with considerable accuracy by both experimental results and by first-principles electronic structure calculations. Fig. 2, therefore, demonstrates that O—B—O bond-angle bending away from the ideal value (~109.47°) of a regular tetrahedron is always present, but subject to stringent geometric constraints [(4), see *Appendix A*]. We therefore conclude that agreement

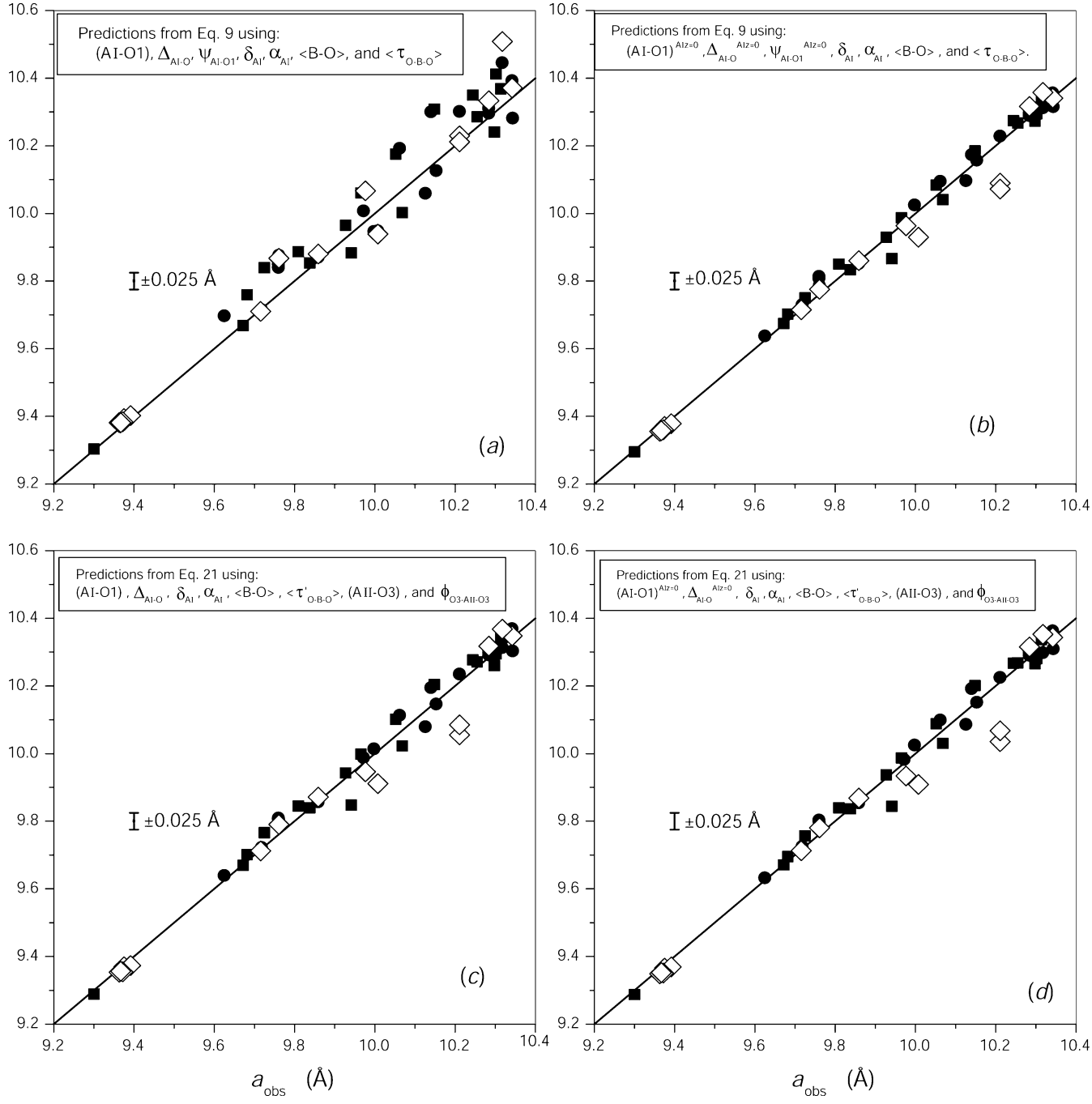

Figure 3
Model predictions made using (*a*), (*b*) equation (2) and (*c*), (*d*) equation (19) of *Appendix A* based on the crystal-chemical parameters in Table 3, as a function of the observed *a* lattice parameter. Filled circles = *ab initio* CO optimizations; filled squares = *ab initio* CC optimizations; open diamonds = single-crystal refinements with agreement factors $R \leq 4.0\%$.

with the relationship illustrated in Fig. 2 is a useful validation criterion during the structure refinement.

3.1.2. Zero value for $z(A^{\rm I})$. The experimental displacement of $A^{\rm I}$ from the z = 0 plane never reaches 0.07 Å (Table 2), which is near the experimental error on this value. This is also true for all but one quantum simulation for $Cd_{10}(PO_4)_6Cl_2$, which predicts a 0.10 Å offset. It should be noted that this simulation, which was started from the atomic coordinates of Sudarsanan *et al.* (1973) and places Cl in Wyckoff position 2(*a*), is questionable as much lower energies were calculated when placing Cl in the Wyckoff position 2(*b*) (Table 2): $E_{\rm total}$ = from −234.23 to −234.88 eV for Cl in 2(*a*) *versus* from −236.16 to −236.2 eV for Cl in 2(*b*). These more reasonable simulations place $A^{\rm I}$ at ∼ 0.02 Å from the z = 0 plane. Simple bond-valence considerations at Cl also lead to the conclusion that Cl is much more likely to be in the Wyckoff position 2(*b*) than in 2(*a*). We conclude that the constraint z = 0 for $A^{\rm I}$ is satisfied within experimental accuracy for all experiments and all valid *ab initio* simulations.

3.2. Comparison of unit-cell parameters with their values recalculated from the model

The values of *a* and *c* are not among the crystal-chemical parameters, but they can be recalculated using several formulae given in *Appendix A*. To the extent that tetrahedral *B*—O bond-stretching and non-uniform O—*B*—O bond-bending distortions can be ignored, all formulae should lead to the same values of *a* and *c* within experimental accuracy.

3.2.1. Predictions of *a* from crystal-chemical parameters. Fig. 3 shows the lattice-parameter predictions for the reconstructed *a* value using (9) and (21) (see *Appendix A*) based on the crystal-chemical parameters compiled in Table 3 as a function of the observed *a* value ($a_{\rm obs}$ displayed on the *x* axis). The predictions are derived from the following crystal-chemical parameters obtained using the equations given in Table 1(*b*): ($A^{\rm I}$—O1) is the length of the three $A^{\rm I}$—O1 bonds in a given $A^{\rm I}O_6$ polyhedron; $(A^{\rm I}{-}{\rm O1})^{A^{\rm I}z=0}$ is the length that the three $A^{\rm I}$—O1 bonds would have if $A^{\rm I}z$ = 0 (Table 1);

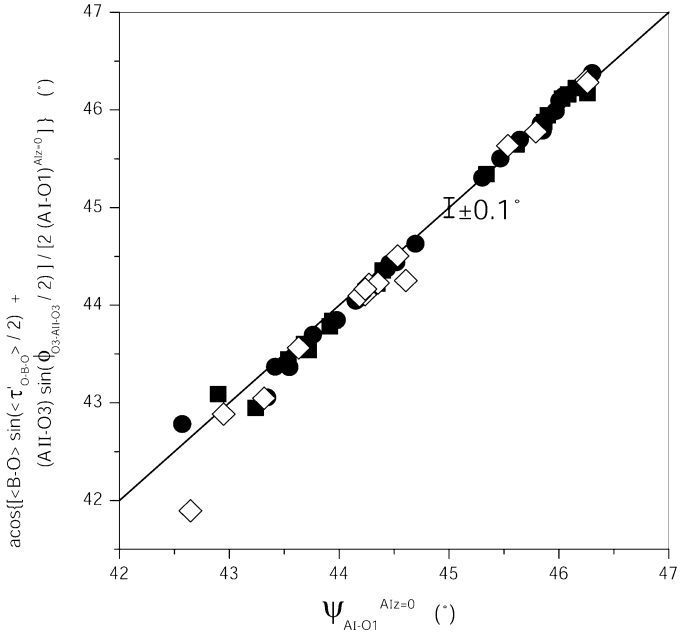

Figure 4
Predicted values of $\psi_{A^{\rm I}-{\rm O1}}^{A^{\rm I}z=0}$ based on equation (20) (*Appendix A*) *versus* those obtained using the equation given in Table 1(*b*). The symbols are as given in Fig. 3.

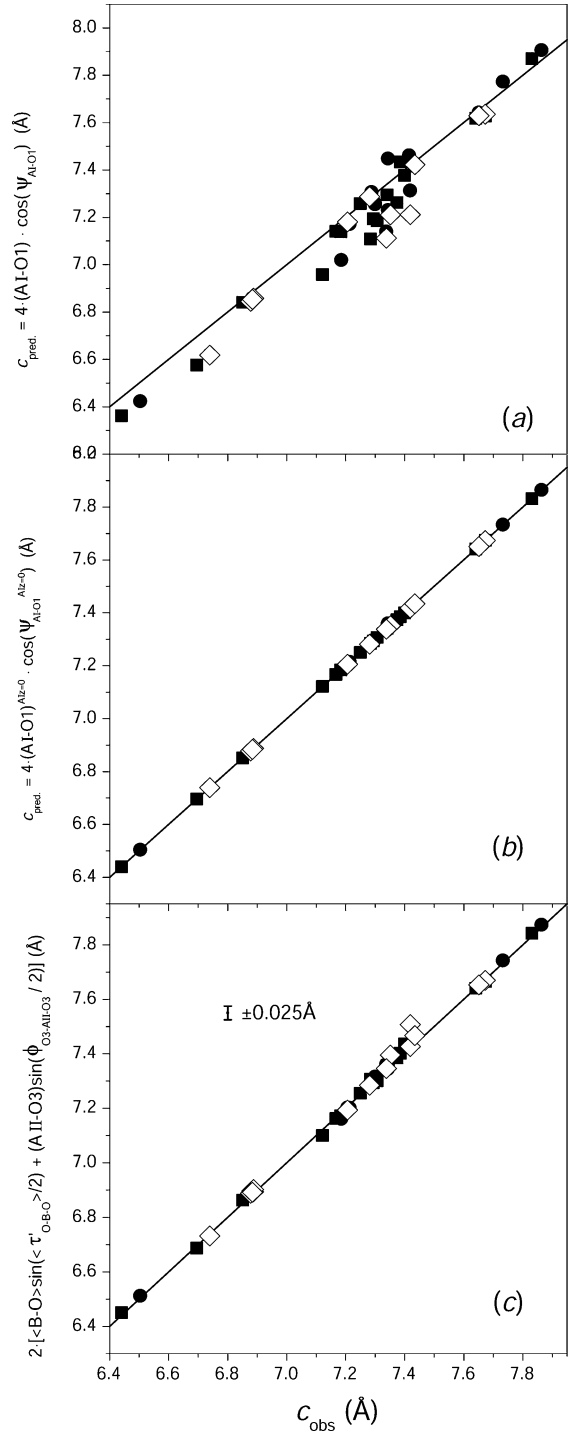

Figure 5
Model predictions made using (*a*), (*b*) equation (2) and (*c*) equation (19) of *Appendix A*, as a function of the observed *c* lattice parameter. The symbols are as given in Fig. 3.

$\Delta_{A^{\rm I}-{\rm O}} = (A^{\rm I}-{\rm O2}) - (A^{\rm I}-{\rm O1})$, where $(A^{\rm I}-{\rm O2})$ is the length of the three $A^{\rm I}-{\rm O2}$ bonds in a given $A^{\rm I}{\rm O}_6$ polyhedron; $\Delta_{A^{\rm I}-{\rm O}}^{A^{\rm I}z=0} = (A^{\rm I}-{\rm O2})^{A^{\rm I}z=0} - (A^{\rm I}-{\rm O1})^{A^{\rm I}z=0}$, where $(A^{\rm I}-{\rm O2})^{A^{\rm I}z=0}$ is the length that the three $A^{\rm I}-{\rm O2}$ bonds would have if $A^{\rm I}z = 0$; $\psi_{A^{\rm I}-{\rm O1}}$ is the angle that the $A^{\rm I}-{\rm O1}$ bonds make with respect to c; $\psi_{A^{\rm I}-{\rm O1}}^{A^{\rm I}z=0}$ is the angle that the $A^{\rm I}-{\rm O1}$ bonds would make with respect to c if $A^{\rm I}z = 0$; $\delta_{A^{\rm I}}$ is the counter-rotation angle of $A^{\rm I}{\rm O}_6$ polyhedra; $\alpha_{A^{\rm I}}$ is the orientation of the $A^{\rm I}{\rm O}_6$ polyhedra with respect to a; $\langle B-{\rm O}\rangle$ is the average of the four bond lengths in any given $B{\rm O}_4$ tetrahedron ($\langle {\rm B}-{\rm O}\rangle = 1/4\cdot[(B-{\rm O1}) + (B-{\rm O2}) + 2\cdot(B-{\rm O3})]$); $\langle\tau_{{\rm O}-B-{\rm O}}\rangle$ is the average of the three ${\rm O}-B-{\rm O}$ bond angles specified by (1*a*); $\langle\tau'_{{\rm O}-B-{\rm O}}\rangle$ is the average of the three ${\rm O}-B-{\rm O}$ bond angles specified by (1*b*); $(A^{\rm II}-{\rm O3})$ is the length of the $A^{\rm II}-{\rm O3}$ bonds within a chain of $\ldots-A^{\rm II}$–O3–B–O3–$A^{\rm II}-\cdots$ atoms (Fig. 1*e*); and $\phi_{{\rm O3}-A^{\rm II}-{\rm O3}}$ is the value of the ${\rm O3}-A^{\rm II}-{\rm O3}$ bond angle in the same chain.

As can be ascertained from the scatter of the data points displayed on the four plots shown in Fig. 3, a better agreement is obtained for cases (Figs. 3*b* and *d*) where model predictions are based on crystal-chemical parameters assuming $z(A^{\rm I}) = 0$ compared with those that do not (Figs. 3*a* and *c*). As the constraint of zero value for $z(A^{\rm I})$ is expected to hold within experimental error (§3.1.2), the larger scatter observed for Figs. 3(*a*) and (*c*) is thus an artifact which can be avoided by

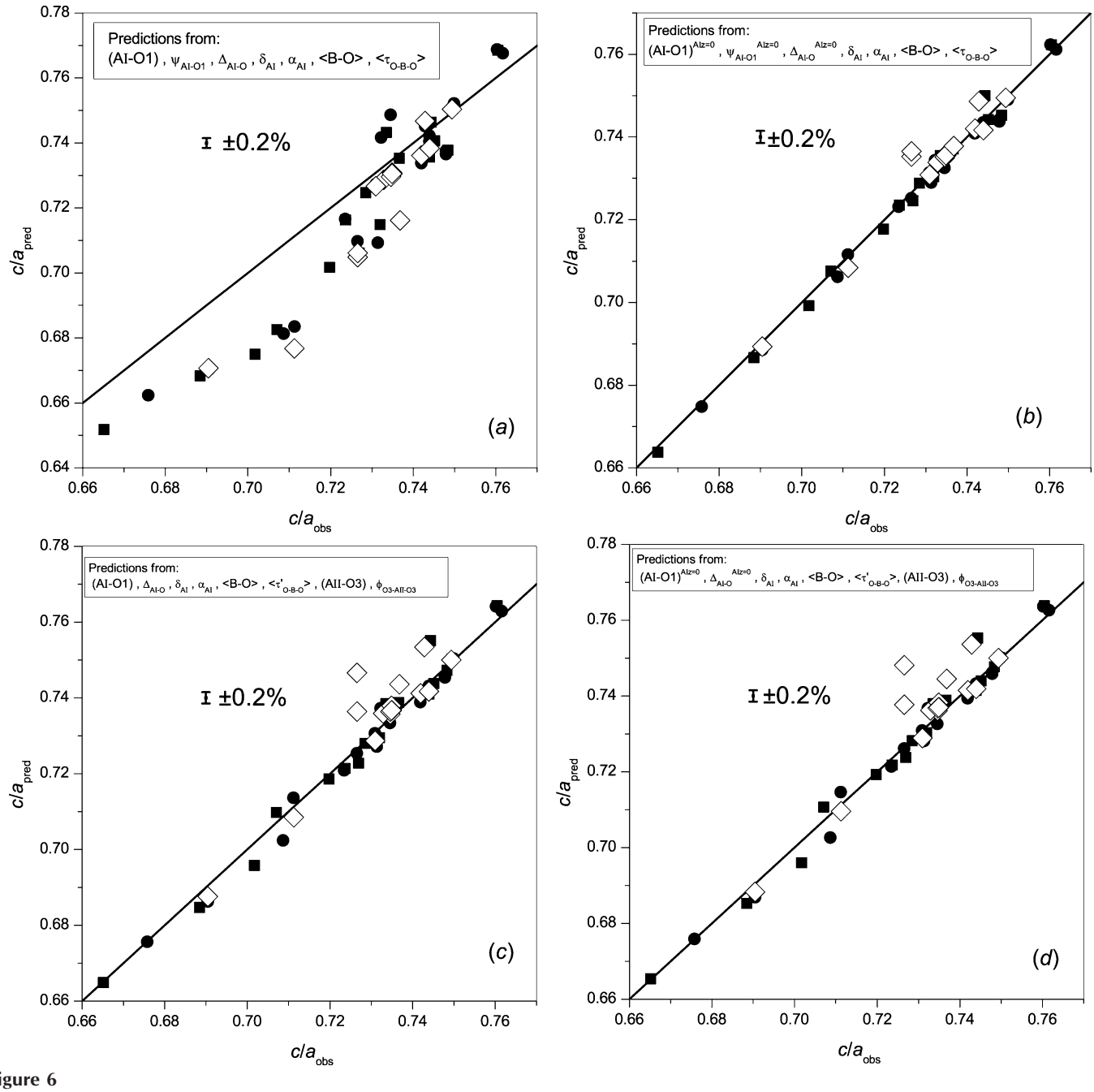

Figure 6
Model predictions made from (*a*), (*b*) equations (2) and (9), and (*c*), (*d*) equations (19) and (21) of *Appendix A*, as a function of the observed *c*/*a* ratio. The symbols are as given in Fig. 3.

Table 4
Results of *ab initio* cell-and-coordinate optimizations for eco-apatite compositions.

(*a*) Electronic energy, unit-cell parameters and fractional atomic coordinates.

Composition	E_{total} (eV per unit cell)	a (Å)	c (Å)	$A^{I}z$	$A^{II}x$	$A^{II}y$	Bx	By	O1x	O1y	O2x	O2y	O3x	O3y	O3z	Xz
$Zn_5(PO_4)_3F$	−244.438	9.1513	5.8445	0.0020	−0.0313	0.2165	0.3975	0.3759	0.3500	0.5130	0.5938	0.4562	0.3259	0.2537	0.0427	0.25
$Zn_5(PO_4)_3F$	−242.455	9.2094	5.7429	0.0016	−0.0359	0.2085	0.4001	0.3783	0.3532	0.5145	0.5946	0.4566	0.3284	0.2558	0.0396	0
$Zn_5(PO_4)_3Cl$	−238.450	9.2982	5.8561	0.0047	−0.0416	0.2279	0.4077	0.3839	0.3602	0.5187	0.6021	0.4613	0.3417	0.2662	0.0404	0
$Zn_5(PO_4)_3Cl$	−240.506	9.2458	5.9468	0.0050	−0.0353	0.2388	0.4038	0.3802	0.3570	0.5169	0.5999	0.4596	0.3384	0.2632	0.0432	0.25
$Hg_5(PO_4)_3Cl$	−210.053	9.6921	6.7772	0.0009	0.0085	0.2684	0.3970	0.3699	0.3352	0.4906	0.5856	0.4610	0.3415	0.2603	0.0666	0.25
$Hg_5(PO_4)_3Cl$	−209.152	9.6971	6.6593	0.0005	0.0006	0.2476	0.4008	0.3740	0.3329	0.4887	0.5882	0.4669	0.3459	0.2621	0.0638	0
$Hg_5(PO_4)_3F$	−213.360	9.5497	6.7393	−0.0017	0.0099	0.2512	0.3902	0.3661	0.3257	0.4868	0.5805	0.4605	0.3301	0.2524	0.0669	0.25
$Hg_5(PO_4)_3F$	−212.360	9.5759	6.6006	−0.0030	0.0029	0.2309	0.3920	0.3696	0.3236	0.4857	0.5809	0.4644	0.3319	0.2538	0.0640	0
$Cd_{10}(VO_4)_6Cl_2$	−253.520	9.7951	6.5788	0.0033	−0.0188	0.2320	0.4112	0.3769	0.3473	0.5095	0.6180	0.4743	0.3440	0.2565	0.0391	0
$Cd_{10}(VO_4)_6Cl_2$	−254.270	9.7943	6.6704	0.0049	−0.0127	0.2513	0.4066	0.3729	0.3455	0.5088	0.6143	0.4686	0.3402	0.2529	0.0438	0.25
$Ca_{10}(VO_4)_6Cl_2$	−315.637	9.8715	6.7600	0.0034	−0.0189	0.2395	0.4127	0.3781	0.3461	0.5071	0.6157	0.4736	0.3505	0.2555	0.0478	0
$Ca_{10}(VO_4)_6Cl_2$	−315.399	9.9034	6.8531	0.0052	−0.0143	0.2594	0.4082	0.3717	0.3510	0.5097	0.6099	0.4630	0.3472	0.2505	0.0497	0.25
$Cd_{10}(CrO_4)_6Cl_2$	−242.830	9.7690	6.5793	0.0031	−0.0172	0.2347	0.4104	0.3790	0.3417	0.5060	0.6135	0.4728	0.3465	0.2578	0.0428	0
$Cd_{10}(CrO_4)_6Cl_2$	−243.589	9.7659	6.6779	0.0046	−0.0123	0.2540	0.4039	0.3728	0.3383	0.5029	0.6079	0.4665	0.3436	0.2533	0.0454	0.25
$Ca_{10}(CrO_4)_6Cl_2$	−303.009	9.8245	6.7134	0.0017	−0.0192	0.2399	0.4120	0.3781	0.3472	0.5073	0.6144	0.4733	0.3536	0.2563	0.0477	0
$Ca_{10}(CrO_4)_6Cl_2$	−302.685	9.8664	6.7777	0.0026	−0.0142	0.2592	0.4069	0.3711	0.3522	0.5086	0.6080	0.4636	0.3517	0.2507	0.0495	0.25
$Pb_{10}(CrO_4)_6Cl_2$	−279.899	10.3035	7.1712	0.0040	−0.0156	0.2415	0.4099	0.3818	0.3335	0.4951	0.6039	0.4797	0.3605	0.2662	0.0604	0
$Pb_{10}(CrO_4)_6Cl_2$	−278.942	10.3337	7.2584	0.0062	−0.0009	0.2677	0.4033	0.3671	0.3336	0.4861	0.5971	0.4628	0.3544	0.2514	0.0631	0.25

(*b*) Crystal-chemical parameters extracted from the crystallographic parameters using the equations given in Table 1(*b*)

Composition	$(A^{I}-O1)$ (Å)	$(A^{I}-O1)^{A^{I}z=0}$ (Å)	$\Delta_{A^{I}-O}$ (Å)	$\Delta^{A^{I}z=0}_{A^{I}-O}$ (Å)	$\psi_{A^{I}-O1}$ (°)	$\psi^{A^{I}z=0}_{A^{I}-O1}$ (°)	$\delta_{A^{I}}$ (°)	$\varphi_{A^{I}}$ (°)	$\alpha_{A^{I}}$ (°)	$\langle B-O\rangle$ (Å)	$\langle\tau_{O-B-O}\rangle$ (°)	$\rho_{A^{II}}$ (Å)	$(A^{II}-X)$ (Å)	$\alpha_{A^{II}}$ (°)	$(A^{II}-O3)$ (Å)	$\phi_{O3-A^{II}-O3}$ (°)
$Zn_5(PO_4)_3F$	2.0776	2.0858	0.0733	0.0571	45.763	45.532	21.735	16.530	−16.657	1.5480	112.590	3.7053	2.1392	126.661	1.9691	120.643
$Zn_5(PO_4)_3F$	2.0706	2.0772	0.0674	0.0545	46.464	46.275	22.342	15.316	−16.273	1.5482	112.858	3.6464	2.5482	127.822	1.9697	115.201
$Zn_5(PO_4)_3Cl$	2.0889	2.1080	0.0825	0.0446	46.557	46.013	24.479	11.041	−16.272	1.5507	113.003	4.0467	2.7572	128.248	2.0115	115.445
$Zn_5(PO_4)_3Cl$	2.0959	2.1166	0.0864	0.0454	45.953	45.379	23.662	12.676	−16.428	1.5502	112.751	4.1367	2.3883	126.800	1.9973	121.575
$Hg_5(PO_4)_3Cl$	2.4069	2.4110	0.0447	0.0366	45.451	45.352	18.934	22.131	−18.416	1.5588	111.888	4.4355	2.5608	118.406	2.2586	143.555
$Hg_5(PO_4)_3Cl$	2.3945	2.3966	0.0602	0.0561	46.051	46.000	19.201	21.598	−19.329	1.5588	112.189	4.1538	2.9194	119.873	2.2711	133.925
$Hg_5(PO_4)_3F$	2.3891	2.3810	0.0505	0.0665	44.763	44.958	17.097	25.806	−19.239	1.5581	111.407	4.0747	2.3525	118.002	2.2496	143.385
$Hg_5(PO_4)_3F$	2.3743	2.3605	0.0631	0.0901	45.309	45.648	17.064	25.872	−19.810	1.5578	111.713	3.8063	2.7482	119.364	2.2478	134.468
$Cd_{10}(VO_4)_6Cl_2$	2.2875	2.3029	0.0724	0.0419	44.801	44.422	24.951	10.099	−20.740	1.7262	110.979	4.1045	2.8846	123.849	2.1819	121.279
$Cd_{10}(VO_4)_6Cl_2$	2.2937	2.3173	0.0704	0.0232	44.547	43.975	23.989	12.022	−20.309	1.7247	111.379	4.3747	2.5258	122.438	2.1692	129.245
$Ca_{10}(VO_4)_6Cl_2$	2.3401	2.3564	0.0680	0.0355	44.566	44.176	24.451	11.099	−20.646	1.7206	112.495	4.2654	2.9867	123.768	2.2992	122.222
$Ca_{10}(VO_4)_6Cl_2$	2.3521	2.3776	0.0445	−0.0068	44.498	43.898	23.997	12.005	−18.732	1.7245	112.854	4.5767	2.6424	122.662	2.2862	127.894
$Cd_{10}(CrO_4)_6Cl_2$	2.2883	2.3029	0.0798	0.0509	44.778	44.419	23.507	12.985	−20.997	1.7030	112.035	4.1245	2.8941	123.513	2.2011	122.162
$Cd_{10}(CrO_4)_6Cl_2$	2.3072	2.3294	0.0718	0.0276	44.753	44.216	22.052	15.896	−20.569	1.7027	112.442	4.4046	2.5430	122.339	2.1871	128.834
$Ca_{10}(CrO_4)_6Cl_2$	2.3371	2.3451	0.0535	0.0376	44.492	44.300	24.445	11.111	−20.302	1.7052	113.057	4.2549	2.9752	123.816	2.2962	120.977
$Ca_{10}(CrO_4)_6Cl_2$	2.3592	2.3719	0.0204	−0.0053	44.714	44.409	23.953	12.093	−18.390	1.7061	113.645	4.5559	2.6303	122.651	2.2824	125.580
$Pb_{10}(CrO_4)_6Cl_2$	2.4980	2.5184	0.1455	0.1052	45.078	44.613	21.510	16.980	−21.476	1.7130	113.457	4.4553	3.1354	123.102	2.5206	124.042
$Pb_{10}(CrO_4)_6Cl_2$	2.5727	2.6038	0.0210	−0.0422	46.540	45.822	19.970	20.060	−19.888	1.7149	113.817	4.7996	2.7711	120.164	2.4815	132.657

constraining $z(A^{\rm I})$ to zero in a given structure refinement or *ab initio* optimization.

Based on (20) (see *Appendix A*) and assuming $z(A^{\rm I}) = 0$, Fig. 4 demonstrates that the angle $\psi_{A^{\rm I}-{\rm O1}}^{A^{\rm I}z=0}$ between an $A^{\rm I}-{\rm O1}$ bond and c can be determined within an expected experimental error of $\pm 0.1^\circ$. On the other hand, the magnitude of a can be obtained with an accuracy of ± 0.025 Å using either crystal-chemical parameters describing the $A^{\rm I}{\rm O}_6$ polyhedra and $B{\rm O}_4$ tetrahedra (Figs. 1*a*–*c*) or from crystal-chemical parameters characterizing $\cdots$–$A^{\rm II}$–O3–B–O3–$A^{\rm II}$–$\cdots$ chains (Fig. 1*e*). This (Figs. 3*b* and *d*, and Fig. 4) represents strong evidence that, given an angle $\psi_{A^{\rm I}-{\rm O1}}$ between an $A^{\rm I}-{\rm O1}$ bond and c imposed by the chains of $\ldots$–$A^{\rm II}$–O3–B–O3–$A^{\rm II}$–$\ldots$ atoms in a given channel of the apatite structure (Fig. 1*e*), the a lattice parameter is determined mostly by geometric constraints inherent to the $(A^{\rm I}{\rm O}_6)$–$(B{\rm O}_4)$ polyhedral arrangement (Fig. 1*c*).

3.2.2. Predictions of c from crystal-chemical parameters. Fig. 5 compares the observed values for c ($c_{\rm obs}$ displayed on the x axis) to predictions with (2) and (19) (see *Appendix A*) using the following crystal-chemical parameters (Table 3): $(A^{\rm I}-{\rm O1})$ and $\psi_{A^{\rm I}-{\rm O1}}$ (Fig. 5*a*); $(A^{\rm I}-{\rm O1})^{A^{\rm I}z=0}$ and $\psi_{A^{\rm I}-{\rm O1}}^{A^{\rm I}z=0}$ (Fig. 5*b*); $\langle B-{\rm O}\rangle$, $\langle\tau'_{{\rm O}-B-{\rm O}}\rangle$, $(A^{\rm II}-{\rm O3})$ and $\phi_{{\rm O3}-A^{\rm II}-{\rm O3}}$ (Fig. 5*c*). Again, a better agreement is reached if $z(A^{\rm I}) = 0$ is assumed in model predictions (Figs. 5*b* and *c* compared with Fig. 5*a*). Whereas the exact agreement shown in Fig. 5(*b*) is imposed by the $P6_3/m$ symmetry, one also notes a remarkable agreement (within ± 0.025 Å) between observations and model predictions [see (19)] based on crystal-chemical parameters characterizing the $\cdots$–$A^{\rm II}$–O3–B–O3–$A^{\rm II}$–$\cdots$ chains (Fig. 1*e*). We conclude that the magnitude of c is actually controlled by these chains, which also determines the angle $\psi_{A^{\rm I}-{\rm O1}}$ between an $A^{\rm I}-{\rm O1}$ bond and c (Fig. 4).

3.2.3. c/a as a function of the crystal-chemical parameters. In the hexagonal system, c/a is the only variable axial ratio thus used as a tabulation index in *e.g. Crystal Data Determinative Tables* (Donnay & Ondik, 1972–1983). As axial ratios often correlate with the chemical and physical properties in a given structure type, c/a is then a key parameter of the $P6_3/m$ apatite structure type, extending over a fairly large range from 0.67 to

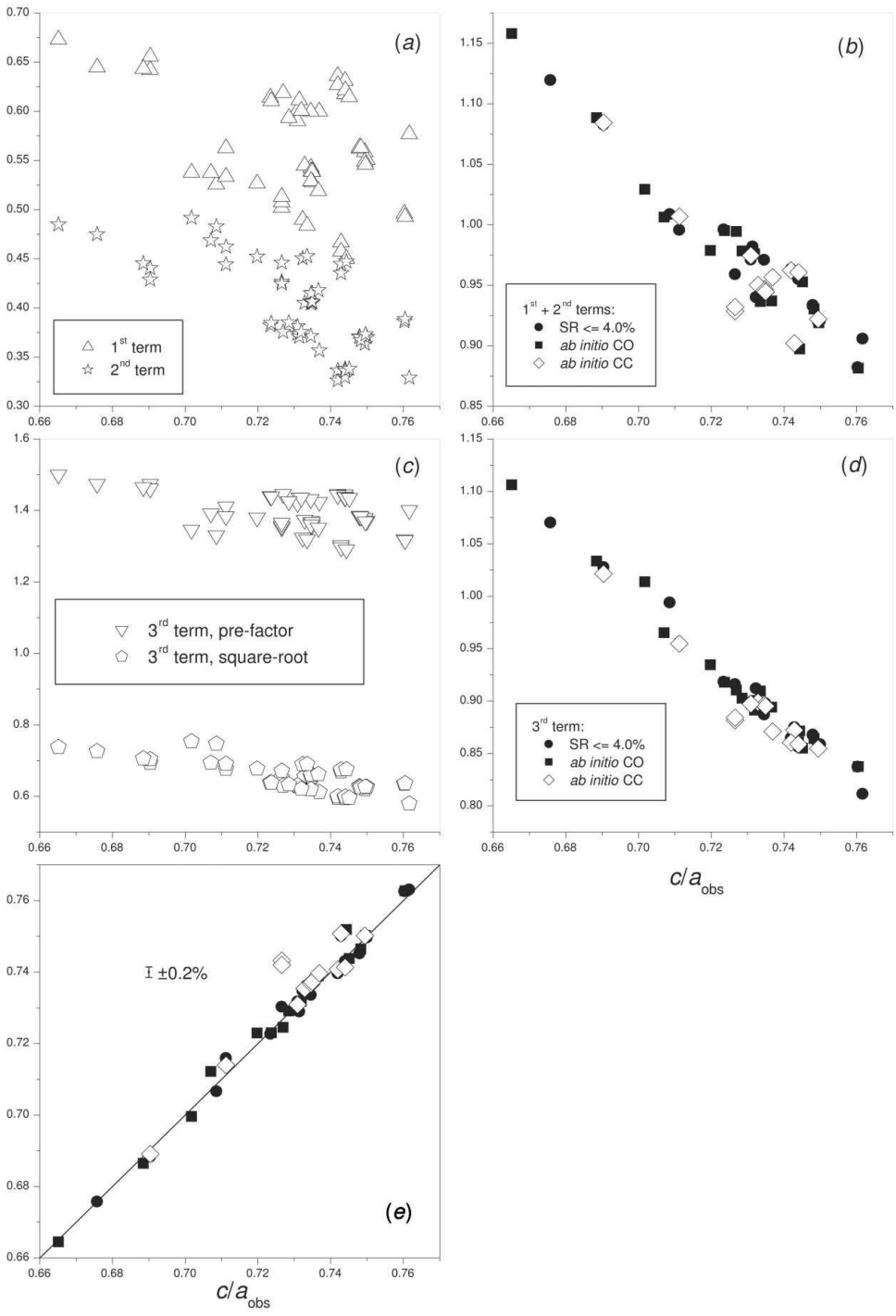

Figure 7
Predictions from equation (10) (*Appendix A*) compared with observed c/a. See text for a detailed explanation of the content of this figure.

0.76 for the $P6_3/m$ apatites in this study.

To ascertain the crystal-chemical dependency of the c/a ratio, Fig. 6 compares the values observed for the c/a ratio, $(c/a)_{obs}$, to the model predictions made from (2), (9), (19) and (21) (see *Appendix A*). Except for a minority of outliers, an agreement within expected experimental error ($\pm 0.2\%$) is obtained between the observations and geometric crystal-chemical predictions made assuming $z(A^{I}) = 0$ (Figs. 6*b* and *d*), for both experimental and *ab initio* optimized structures.

In a similar connection, Fig. 7 compares the observed c/a ratios to model predictions made from (10) (see *Appendix A*). As a function of $(c/a)_{obs}$, the various terms of (10) are plotted (Fig. 7) as follows:

(i) the first and second terms shown separately (Fig. 7*a*);

(ii) the sum of the first and second terms (Fig. 7*b*);

(iii) the multiplying pre-factor and the square-root expression in the third term shown separately (Fig. 7*c*);

(iv) the third term together (Fig. 7*d*);

(v) the overall prediction from (10) (Fig. 7*e*).

Fig. 7 demonstrates that the overall variation of c/a ratios observed in $P6/_3m$ apatites can be reduced to a function of six crystal-chemical parameters, namely: $\langle A^{I}-O\rangle^{A^{I}z=0}$, $\langle\psi_{A^{I}-O}\rangle^{A^{I}z=0}$, $\delta_{A^{I}}$, $\alpha_{A^{I}}$, $\langle B-O\rangle$ and $\langle\tau_{O-B-O}\rangle$ (where $\langle A^{I}-O\rangle^{A^{I}z=0} = (1/2)\cdot[(A^{I}-O1)^{A^{I}z=0} + (A^{I}-O2)^{A^{I}z=0}]$; $\langle\psi_{A^{I}-O}\rangle^{A^{I}z=0} = (1/2)\cdot[\psi^{A^{I}z=0}_{A^{I}-O1} + \psi^{A^{I}z=0}_{A^{I}-O2}]$). By contrast, Fig. 8S (deposited as supplementary material[1]) shows that $\delta_{A^{I}}$ and $\langle\tau_{O-B-O}\rangle$ are the two single crystal-chemical parameters that correlate most with observed c/a ratios, but only weakly in comparison to multi-variable functions based on model geometric crystal-chemical predictions (Figs. 6 and 7).

We conclude that the variation of c/a ratios observed in $P6/_3m$ apatites results from a combination of crystal-chemical factors acting concomitantly and does not arise from a single crystal-chemical parameter.

3.3. *Ab initio versus* experimental data

Fig. 9S (deposited as supplementary material) compares experimental and *ab initio* results for the following quantities:

(i) the a and c lattice parameters (Figs. 9S*a* and *b*);

(ii) the crystal-chemical parameters (Table 3) extracted from the crystallographic descriptions (a, c, atom coordinates; Table 2) using the equations given in Table 1(*b*) (Figs. 9S*b*–*p*);

(iii) the distinct crystallographic $A^{II}-O$ bond lengths – ($A^{II}-O3$), ($A^{II}-O3'$), ($A^{II}-O2$) and ($A^{II}-O1$) – occurring in the $A^{II}O_6X_{1,2}$ polyhedra (Figs. 9S*q*–*t*).

Ab initio and experimental data agree to within ±0.5–2.0% (Fig. 9S); an agreement which is comparable to the precision which can be achieved in routine powder diffraction measurements. The few outliers (*i.e.* falling outside a concordance of $\pm$ 0.5–2.0%) refer to single-crystal determinations with $R > 4.0\%$, Rietveld refinements or energy-prohibited *ab initio* optimizations (Table 2). This suggests that care must be taken to obtain reliable experimental crystal-structure determinations. Indeed, most Rietveld studies (*e.g.* Dong & White, 2004*a*; Kim *et al.*, 2000; Bigi *et al.*, 1989) required the use of bond constraints to obtain reasonable bond lengths for BO_4 tetrahedra (*i.e.* BO_4 bond lengths consistent with $B-O$ distances computed from Shannon's radii). In on-going work (unpublished results), it is shown that the use of geometrical parameterization better controls the least-squares minimization process during Rietveld refinements of powder diffraction data compared with rigid-body or other types of bond constraints.

We conclude that *ab initio* optimizations of apatite crystal structures with given stoichiometry, and degree and type of chemical order should serve as a useful starting point in the search for apatite-type materials with tailored structural and crystal-chemical properties. In this regard, *ab initio* cell-and-coordinate optimizations (Table 4) were also performed for a selection of 'eco-apatite' (White *et al.*, 2005; Dong & White, 2004*a*,*b*; Dong *et al.*, 2002; Kim *et al.*, 2005) compositions relevant to the stabilization of toxic metals (Zn, Hg, V, Cr, Pb, Cd) from industrial wastes such as incinerator fly ashes. Note that an ordering of F is predicted to occur in Wyckoff position 2(*b*) for $Zn_{10}(PO_4)_6F_2$ rather than in 2(*a*) for all other end-member compositions (see Tables 2 and 4). Similarly, an ordering of Cl in 2(*a*) instead of 2(*b*) is predicted for $Hg_{10}(PO_4)_6Cl_2$, $Cd_{10}(VO_4)_6Cl_2$ and $Cd_{10}(CrO_4)_6Cl_2$. Experiments are in progress to determine whether these predicted structures can be synthesized.

3.4. Correlations between polyhedral distortion parameters

Several of the crystal-chemical parameters used in the geometrical parameterization correspond to polyhedral distortions, *e.g.* the uniform bond-angle bending of BO_4 tetrahedra as well as some angles within $A^{I}O_6$ and $A^{II}O_6X_{1,2}$ polyhedra. As these are algebraically independent parameters, it is significant that the plots of $\delta_{A^{I}}$ *versus* $\phi_{O3-A^{II}-O3}$, $\langle\tau_{O-B-O}\rangle$ *versus* $\phi_{O3-A^{II}-O3}$, $\psi^{A^{I}z=0}_{A^{I}-O1}$ *versus* $\alpha_{A^{I}}$ and $\alpha_{A^{II}}$ *versus* $\phi_{O3-A^{II}-O3}$ demonstrate strong correlations (Fig. 8). The crystal-chemical parameters allow sufficient structural flexibility for the apatite structure to accommodate entities that do not fit, not through the distortion of a single parameter, but through cooperative distortions that relieve the stress caused by others to minimize the total energy of the system.

Distortions of the BO_4 tetrahedra and $A^{I}O_6$ polyhedra are observed to correlate with the $A^{II}O_6X_{1,2}$ bond angle $\phi_{O3-A^{II}-O3}$ (Figs. 8*a* and *b*), supporting the crystal-chemical idea that the $\ldots$–A^{II}–O3–B–O3–A^{II}–$\cdots$ chains play a predominant role in determining the overall structure (see Figs. 3 and 4 and their associated discussions). On the other hand, distortion parameters within a given polyhedron self correlate (Figs. 8*c* and *d*), confirming that local stereochemical bonding effects are also significant. The minimum-energy solution (*i.e.* the observed experimental and *ab initio* optimized structures) is thus the result of a compromise between (i) long-range geometric effects related to the misfit of BO_4, $A^{I}O_6$ and $A^{II}O_6X_{1,2}$ building blocks, and (ii) the preferred

[1] Supplementary data for this paper are available from the IUCr electronic archives (Reference: LC5033). Services for accessing these data are described at the back of the journal.

local bonding characteristics of a specific cation within a given coordination polyhedron.

4. Conclusions

Comparing the geometric constraints assumed in the geometrical parameterization and the observed *a* and *c* lattice parameters to model geometric crystal-chemical predictions points towards the following four conclusions.

(i) For fully ordered $P6_3/m$ apatites, the constraints of zero value for the *z* coordinate of $A^{\rm I}$ is satisfied within experimental accuracy for both experimental and *ab initio* optimized structures.

(ii) The BO_4 tetrahedra exhibit a local $3m$ pseudo-symmetry with B—O1 as its axis.

(iii) To an accuracy of $\pm$ 0.025 Å, the magnitude of *c* can be predicted using crystal-chemical parameters characterizing the six chains of $\ldots$–$A^{\rm II}$–O3–B–O3–$A^{\rm II}$–$\cdots$ atoms located in any given channel of the apatite structure, whereas that of *a* can be determined from crystal-chemical parameters describing the $(A^{\rm I}{\rm O}_6)$–$(B{\rm O}_4)$ polyhedral arrangement.

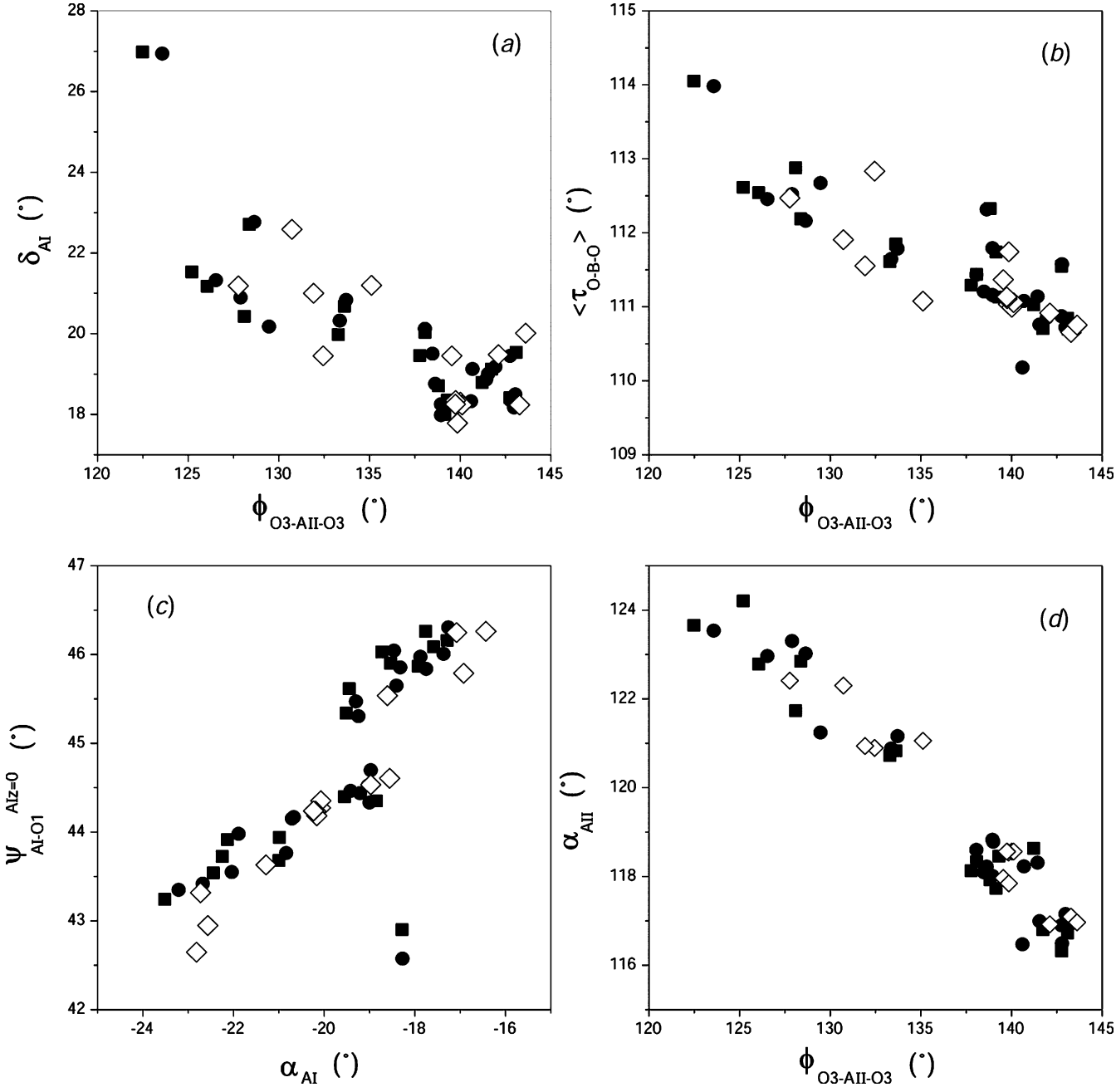

Figure 8
Correlations observed between polyhedral distortion parameters: $\delta_{A^{\rm I}}$ *versus* (*a*) $\phi_{{\rm O3}-A^{\rm II}-{\rm O3}}$, (*b*) $\langle\tau_{{\rm O}-B-{\rm O}}\rangle$ *versus* $\phi_{{\rm O3}-A^{\rm II}-{\rm O3}}$, (*c*) $\phi^{A^{\rm I}z=0}_{A^{\rm I}-{\rm O1}}$ *versus* $\alpha_{A^{\rm I}}$ and (*d*) $\alpha_{A^{\rm II}}$ *versus* $\phi_{{\rm O3}-A^{\rm II}-{\rm O3}}$. The symbols are as given in Fig. 3.

(iv) The c/a ratio can be predicted within an expected experimental error of $\pm 0.2\%$ using multi-variable functions based on geometric crystal-chemical model predictions, but cannot be ascribed to a single crystal-chemical parameter.

Comparison of *ab initio* optimized structures with experimental ones shows good agreement (within ± 0.5–2.0%) for only the most reliable single-crystal refinements. Accordingly, *ab initio* cell data, atomic coordinates and crystal-chemical parameters are reported for a selection of apatite compositions not yet studied experimentally (Table 4). Finally, the observed correlations between algebraically independent crystal-chemical parameters representing polyhedral distortions reveal them to be the minimum-energy solution to accommodate misfit components within the flexible $P6_3/m$ apatite structure type.

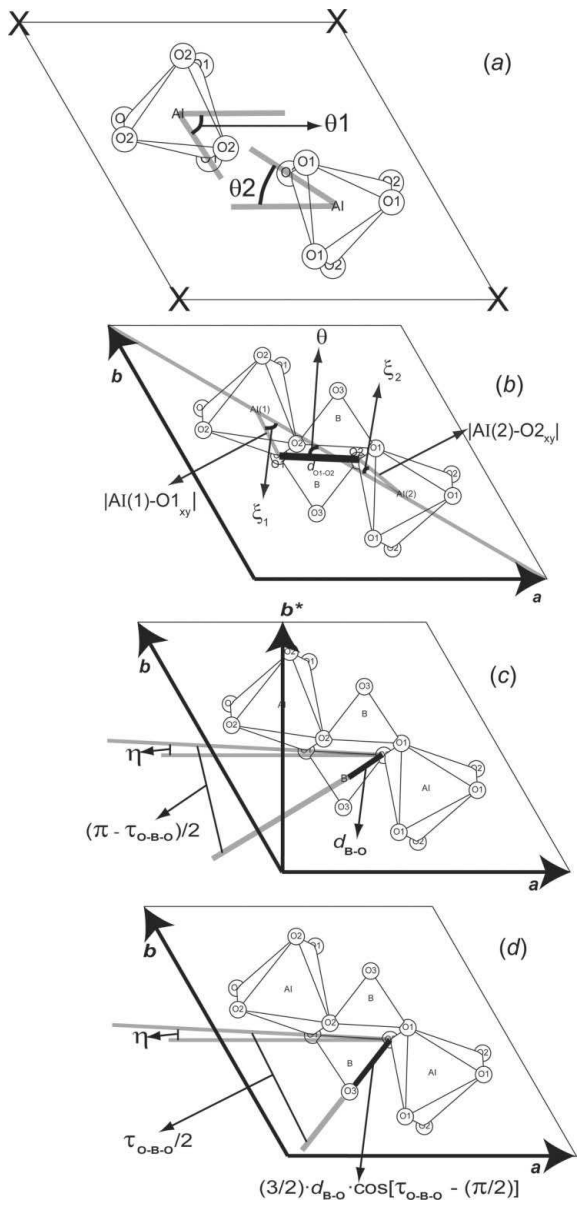

Figure 9
Geometric constructions used to: (*a*) obtain values of $\delta_{A^{\rm I}}$ and $\alpha_{A^{\rm I}}$ from the crystallographic description (see Table 1*b* and associated text); (*b*) derive an expression for the magnitude of the lattice parameter *a*; and derive fractional atomic coordinates for (*c*) *B* and (*d*) O3 Wyckoff positions.

Compared to the usual crystal structure representations that consist of space-group symmetry information, unit-cell parameters and fractional atomic coordinates, the analysis of structure types in terms of crystal-chemical parameters provides a theoretical framework more 'transparent to chemical and physical intuition' (Hawthorne, 1994) than the independent crystallographic parameters. The geometric crystal-chemical model of $P6_3/m$ apatite developed in this paper summarizes the main polyhedral distortions observed in apatite-type materials *via* convenient crystal-chemical parameters. Presumably, the observed polyhedral distortions are related to internal strains connected with the presence of chemical composition differences from one unit cell to another in the crystal and to synthesis or re-equilibration conditions. As our geometric approach provides detailed theoretical predictions against which the structural properties of real apatite samples can be analyzed, it should be helpful in correlating observed crystal structures with other measured physical properties.

APPENDIX *A*
Geometrical derivation

A1. $A^{\rm I}O_6$ polyhedra

The $A^{\rm I}$ cations project onto the *ab* plane to form a perfect hexagonal net centered by the *X* anions (Fig. 9*a*) with the $A^{\rm I}$ cations occupying a Wyckoff position of type 4(*f*) with $z = 0$ $(x, y, z = \frac{1}{3}, \frac{2}{3}, z; \frac{2}{3}, \frac{1}{3}, -z; \frac{1}{3}, \frac{2}{3}, -z + \frac{1}{2}; \frac{2}{3}, \frac{1}{3}, z + \frac{1}{2})$. The *X* anion columns run parallel to [001].

Next, the positions of the coordinating O1 and O2 atoms around the $A^{\rm I}$ cations are specified using the following crystal-chemical parameters (Figs. 1*a*):

(i) $A^{\rm I}$—O1 bond length, $d_{A^{\rm I}-{\rm O1}}$;

(ii) bond-length difference between $A^{\rm I}$—O1 and $A^{\rm I}$—O2 bonds, $\Delta_{A^{\rm I}-{\rm O}}$;

(iii) angle that an $A^{\rm I}$—O1 bond makes with respect to *c*, $\psi_{A^{\rm I}-{\rm O1}}$;

(iv) counter-rotation angle of the $A^{\rm I}O_6$ polyhedra, $\delta_{A^{\rm I}}$;

(v) orientation of the $A^{\rm I}O_6$ polyhedra with respect to *a*, $\alpha_{A^{\rm I}}$.

Assuming that O1 and O2 are positioned midway between the $A^{\rm I}$ cation planes located at $z = 0, \pm\frac{1}{2}, \pm 1, \pm\frac{3}{2}$ *etc.*, it follows that their fractional atomic coordinates can be specified by two Wyckoff positions of the type 6(*h*) $(x, y, z = x, y, \frac{1}{4}; -y, x - y, \frac{1}{4}; -x + y, -x, \frac{1}{4}; -x, -y, \frac{3}{4}; y, -x + y, \frac{3}{4}; x - y, x, \frac{3}{4})$ using the bond-length and bond-angle parameters $d_{A^{\rm I}-{\rm O1}}$, $\Delta_{A^{\rm I}-O}$, $\psi_{A^{\rm I}-{\rm O1}}$, $\delta_{A^{\rm I}}$ and $\alpha_{A^{\rm I}}$ (Table 1). It also follows that the *c* lattice parameter is given by

$$c = 4d_{A^{\rm I}-{\rm O1}}\cos(\psi_{A^{\rm I}-{\rm O1}}). \qquad (2)$$

In the present model, the same symmetry constraints that are imposed during structure refinement in $P6_3/m$ with O1 and O2 in 6(*h*) positions are adopted here in the geometric

representation of $A^{\rm I}O_6$ polyhedra. However, cation-centered $A^{\rm I}O_6$ polyhedra are idealized by imposing $z = 0$ for the $A^{\rm I}$ cations in the Wyckoff position 4(*f*) (Table 1).

A2. BO_4 tetrahedra

A single bond length $d_{B-{\rm O}}$ is specified for all $B-{\rm O}$ bonds, but the tetrahedral shape is allowed to vary through bending of the ${\rm O}-B-{\rm O}$ bond angles (Fig. 1*b*). This is accomplished (Fig. 1*c*) by positioning the B cations at an equal distance $d_{B-{\rm O}}$ from their nearest-neighbour O1 and O2 atoms onto planes at $z = \pm\frac{1}{4}, \pm\frac{3}{4}$ *etc.*, where an ${\rm O1}-B-{\rm O2}$ bond angle of a certain value $\tau_{{\rm O}-B-{\rm O}}$ is also specified. Thus, the B cations can be fixed at a Wyckoff position of the type 6(*h*). The O3 atoms are then inserted into the 12(*i*) Wyckoff position so that distinct crystallographic $\tau({\rm O}i-{\rm B}-{\rm O}i)$ angles (Fig. 1*b*) are given by the following expressions (where bond angle multiplicities are given in square brackets)

$$\tau({\rm O1}-B-{\rm O2})[\times 1] = \tau({\rm O1}-B-{\rm O3})[\times 2] \equiv \tau_{{\rm O}-B-{\rm O}} \quad (3a)$$

$$\tau({\rm O2}-B-{\rm O3})[\times 2] = \tau({\rm O3}-B-{\rm O3}')[\times 1] \equiv \tau'_{{\rm O}-B-{\rm O}} \quad (3b)$$

where

$$\tau'_{{\rm O}-B-{\rm O}} = 2\arcsin\{(3^{1/2}/2)\cos[\tau_{{\rm O}-B-{\rm O}} - (\pi/2)]\}. \quad (4)$$

In the present model, therefore, the BO_4 tetrahedra are fully defined by two crystal-chemical parameters: the bond length $d_{B-{\rm O}}$ and the bond-bending angle $\tau_{{\rm O}-B-{\rm O}}$. Fractional atomic coordinates for B and O3 atoms are derived below, after an expression for the lattice parameter a is obtained.

Consider more closely the structural arrangement of $A^{\rm I}O_6$ and BO_4 polyhedra (Fig. 9*b*). The distance between the two labelled $A^{\rm I}$ cations – $A^{\rm I}(1)$ and $A^{\rm I}(2)$ (Fig. 9*b*) – must equal $a/(3^{1/2})$. Moreover, given the model crystal-chemical parameters assumed for $A^{\rm I}O_6$ polyhedra (Fig. 1*a*; Table 1), it follows that:

(i) the projections of the labelled $A^{\rm I}(1)-{\rm O1}$ and $A^{\rm I}(2)-{\rm O2}$ bonds onto the *ab*-plane, $A^{\rm I}(1)-{\rm O1}_{xy}$ and $A^{\rm I}(2)-{\rm O2}_{xy}$, are of lengths

$$|A^{\rm I}(1)-{\rm O1}_{xy}| = d_{A^{\rm I}-{\rm O1}}\sin(\psi_{A^{\rm I}-{\rm O1}}) \quad (5a)$$

$$|A^{\rm I}(2)-{\rm O2}_{xy}| = 3^{1/2}(d_{A^{\rm I}-{\rm O1}} + \Delta_{A^{\rm I}-{\rm O}}) \times \{1 - [\cos^2(\psi_{A^{\rm I}-{\rm O1}})]/[1 + (\Delta_{A^{\rm I}-{\rm O}}/d_{A^{\rm I}-{\rm O1}})]^2\}^{1/2} \quad (5b)$$

and

(ii) the in-plane angles ξ_1 and ξ_2 (Fig. 9*b*) have the following values

$$\xi_1 = (\pi/6) - \delta_{A^{\rm I}} - \alpha_{A^{\rm I}} \quad (6a)$$

$$\xi_2 = (\pi/6) - \delta_{A^{\rm I}} + \alpha_{A^{\rm I}}. \quad (6b)$$

The distance between the labelled O1 and O2 atoms, $d_{{\rm O1}-{\rm O2}}$ (Fig. 9*b*), is readily obtained from the BO_4 model parameters (Figs. 1*b* and *c*) as

$$d_{{\rm O1}-{\rm O2}} = 2d_{B-{\rm O}}\sin(\tau_{{\rm O}-B-{\rm O}}/2). \quad (7)$$

Upon further examination of this geometric construction (Fig. 9*b*), it is now clear that

$$a/(3^{1/2}) = |A^{\rm I}(1) - {\rm O1}_{xy}|\cos(\xi_1) + |A^{\rm I}(2)-{\rm O2}_{xy}|\cos(\xi_2) + d_{{\rm O1}-{\rm O2}}\cos(\theta), \quad (8)$$

where the angle θ is defined in Fig. 9(*b*). By substitution of (5), (6) and (7) into (8), the lattice parameter a can be expressed as

$$a = 3^{1/2}d_{A^{\rm I}-{\rm O1}}\sin(\psi_{A^{\rm I}-{\rm O1}})\cos[(\pi/6) - \delta_{A^{\rm I}} - \alpha_{A^{\rm I}}] + 3^{1/2}(d_{A^{\rm I}-{\rm O1}} + \Delta_{A^{\rm I}-{\rm O}})\{1 - [\cos^2(\psi_{A^{\rm I}-{\rm O1}})]/[1 + (\Delta_{A^{\rm I}-{\rm O}}/d_{A^{\rm I}-{\rm O1}})]^2\}^{1/2}\cos[(\pi/6) - \delta_{A^{\rm I}} + \alpha_{A^{\rm I}}] + 2(3^{1/2})d_{B-{\rm O}}\sin(\tau_{{\rm O}-B-{\rm O}}/2)\cos(\theta), \quad (9a)$$

where

$$\sin(\theta) = \{d_{A^{\rm I}-{\rm O1}}\sin(\psi_{A^{\rm I}-{\rm O1}})\sin[(\pi/6) - \delta_{A^{\rm I}} - \alpha_{A^{\rm I}}] - (d_{A^{\rm I}-{\rm O1}} + \Delta_{A^{\rm I}-{\rm O}})\{1 - [\cos^2(\psi_{A^{\rm I}-{\rm O1}})]/[1 + (\Delta_{A^{\rm I}-{\rm O}}/d_{A^{\rm I}-{\rm O1}})]^2\}^{1/2}\sin[(\pi/6) - \delta_{A^{\rm I}} + \alpha_{A^{\rm I}}]\}/[2d_{B-{\rm O}}\sin(\tau_{{\rm O}-B-{\rm O}}/2)]. \quad (9b)$$

Note that if $d_{A^{\rm I}-O} = d_{A^{\rm I}-{\rm O1}} = d_{A^{\rm I}-{\rm O2}}$ and $\psi_{A^{\rm I}-{\rm O}} = \psi_{A^{\rm I}-{\rm O1}} = \psi_{A^{\rm I}-{\rm O2}}$, then the c/a axial ratio can be obtained from the following equation [obtained after dividing (2) by (9), assuming $\Delta_{A^{\rm I}-{\rm O}} = 0$ and rearranging the terms]

$$[1/(c/a)]^2 = (3/4)\cdot\tan^2(\psi_{A^{\rm I}-{\rm O}})\cdot\cos^2(\pi/6 - \delta_{A^{\rm I}})\cdot\cos(2\cdot\alpha_{A^{\rm I}}) + (3/4)\cdot[d_{B-{\rm O}}\cdot\sin(\tau_{{\rm O}-B-{\rm O}}/2)]^2/[d_{A^{\rm I}-{\rm O}}\cdot\cos(\psi_{A^{\rm I}-{\rm O}})]^2 + (3/2)\cdot\tan(\psi_{A^{\rm I}-{\rm O}})\cdot\cos(\pi/6 - \delta_{A^{\rm I}})\cdot\cos(\alpha_{A^{\rm I}})\cdot\{[d_{B-{\rm O}}\cdot\sin(\tau_{{\rm O}-B-{\rm O}}/2)]^2/[d_{A^{\rm I}-{\rm O}}\cdot\cos(\psi_{A^{\rm I}-{\rm O}})]^2 - \tan^2(\psi_{A^{\rm I}-{\rm O}})\cdot\cos^2(\pi/6 - \delta_{A^{\rm I}})\cdot\cos^2(\alpha_{A^{\rm I}})\cdot\sin^2(\alpha_{A^{\rm I}})\}^{1/2}. \quad (10)$$

To derive the fractional atomic coordinates for the B and O3 sites (Table 1) consider Figs. 9(*c*) and (*d*). The distances and angles indicated on the lower BO_4 tetrahedron of these two geometric constructions correspond to the geometric model BO_4 representation [see (3) and (4); Fig. 1*b*], measured with respect to a projection onto the *ab* plane. From these, the following orthogonal (trimetric) atomic coordinates are obtained for B (Fig. 9*c*) and O3 (Fig. 9*d*)

$$Bx_{\rm ortho} = {\rm O2}x_{\rm ortho} - d_{B-{\rm O}}\cos[(\pi - \tau_{{\rm O}-B-{\rm O}})/2 + \eta] \quad (11a)$$

$$By_{\rm ortho} = {\rm O2}y_{\rm ortho} - d_{B-{\rm O}}\sin[(\pi - \tau_{{\rm O}-B-{\rm O}})/2 + \eta] \quad (11b)$$

$${\rm O3}x_{\rm ortho} = {\rm O2}x_{\rm ortho} - (3/2)d_{B-{\rm O}}\cos[\tau_{{\rm O}-B-{\rm O}} - (\pi/2)] \times \cos[(\tau_{{\rm O}-B-{\rm O}}/2) + \eta] \quad (12a)$$

$${\rm O3}y_{\rm ortho} = {\rm O2}y_{\rm ortho} - (3/2)d_{B-{\rm O}}\cos[\tau_{{\rm O}-B-{\rm O}} - (\pi/2)] \times \sin[(\tau_{{\rm O}-B-{\rm O}}/2) + \eta], \quad (12b)$$

where ${\rm O2}x_{\rm ortho}$ and ${\rm O2}y_{\rm ortho}$ are the (x, y) orthogonal coordinates of the O2 atom. These orthogonal coordinates (${\rm O2}x_{\rm ortho}$, ${\rm O2}y_{\rm ortho}$, $Bx_{\rm ortho}$, $By_{\rm ortho}$, ${\rm O3}x_{\rm ortho}$ and ${\rm O3}y_{\rm ortho}$)

correspond to a Cartesian system along the a, b^* and c axes (Fig. 9c). The values of $O2x_{ortho}$ and $O2y_{ortho}$ are obtained as

$$O2x_{ortho} = a \cdot [x(O2) - (1/2) \cdot y(O2)] \quad (13a)$$

$$O2y_{ortho} = a \cdot [3^{1/2} \cdot y(O2)]/2, \quad (13b)$$

where $x(O2)$ and $y(O2)$ are the hexagonal $P6_3/m$ fractional atomic coordinates listed in Table 1 and the lattice parameter a is determined from (9) [or (21)]. The value of the angle η [(11) and (12); Figs. 9c and d] is given by

$$\tan(\eta) = [O1y_{ortho} - O2y_{ortho}]/[O1x_{ortho} - O2x_{ortho}], \quad (14)$$

where $O1x_{ortho}$ and $O1y_{ortho}$ are derived as in (13) for $O2x_{ortho}$ and $O2y_{ortho}$.

Using (11)–(14), the (x, y) fractional atomic coordinates for B and O3 (Table 1) are written as

$$x(B) = [Bx_{ortho}/a] + [By_{ortho}/(3^{1/2}a)] \quad (15a)$$

$$y(B) = [2 \cdot By_{ortho}/(3^{1/2}a)] \quad (15b)$$

$$x(O3) = [O3x_{ortho}/a] + [O3y_{ortho}/(3^{1/2}a)] \quad (16a)$$

$$y(O3) = [2 \cdot O3y_{ortho}/(3^{1/2}a)]. \quad (16b)$$

The z coordinate of O3 (Table 1), by inspection of Fig. 1(b), is readily obtained as

$$z(O3) = (1/4) - [d_{B-O} \sin(\tau'_{O-B-O}/2)]/c, \quad (17)$$

where τ'_{O-B-O} is given by (4) and c follows from (2) [or (19)].

A3. $A^{II}O_6X_{1,2}$ polyhedra

The model of the crystal structure is completed by specifying the positions of A^{II} cations and X anions inside [001] channels that are formed within the $(A^{I}O_6)$–(BO_4) polyhedral network (Fig. 1c). For this purpose, five additional crystal-chemical parameters are defined (Figs. 1d and e):

(i) the A^{II}–A^{II} triangular side length, $\rho_{A^{II}}$;

(ii) the orientation of equilateral A^{II}–A^{II}–A^{II} triangles with respect to a, $\alpha_{A^{II}}$;

(iii) the A^{II}—X bond length, $d_{A^{II}-X}$;

(iv) the A^{II}—O3 bond length, $d_{A^{II}-O3}$;

(v) the O3—A^{II}—O3 bond angle, $\phi_{O3-A^{II}-O3}$.

The A^{II} cations are assumed to lie on planes at $z = \pm 1/4$, $\pm 3/4$ *etc.* in equilateral triangles centered about the X-anion columns (Fig. 1d), so that A^{II} cations occupy a Wyckoff position of type 6(h) with (x, y) fractional atomic coordinates expressed in terms of model parameters $\rho_{A^{II}}$ and $\alpha_{A^{II}}$ (Table 1). Depending on whether the X anions occupy Wyckoff positions 2(a) or 2(b), the A^{II}—A^{II} triangular side length $\rho_{A^{II}}$ is given by

$$\text{for } X \text{ in } 2a: \quad \rho_{A^{II}} = 3^{1/2} \cdot d_{A^{II}-X} \quad (18a)$$

$$\text{for } X \text{ in } 2b: \quad \rho_{A^{II}} = 3^{1/2} \cdot [d^2_{A^{II}-X} - (c^2/16)]^{1/2}, \quad (18b)$$

where c is obtained from (2) [or (19)]. Note that only one of these two parameters, $d_{A^{II}-X}$ or $\rho_{A^{II}}$, needs be specified and the other follows.

Alternate expressions for a and c lattice parameters can also be derived involving the A^{II}—O3 bond length $d_{A^{II}-O3}$ and O3—A^{II}—O3 bond angle $\phi_{O3-A^{II}-O3}$ (Fig. 1e). In terms of parameters that characterize $A^{II}O_6X_{1,2}$ and BO_4 polyhedra, Fig. 1(e) shows that c can be expressed as

$$c = 2 \cdot [d_{B-O} \sin(\tau'_{O-B-O}/2) + d_{A^{II}-O3} \sin(\phi_{O3-A^{II}-O3}/2)], \quad (19)$$

where d_{B-O} is the tetrahedral BO_4 bond length (Fig. 1b) and τ'_{O-B-O} is given by (4). Moreover, if we keep the same geometric representation for $A^{I}O_6$ and BO_4 polyhedra (Figs. 1a–c), then the following additional geometric constraint [obtained by equating (2) and (19)] must be obeyed

$$\cos(\psi_{A^{I}-O1}) = [d_{B-O} \sin(\tau'_{O-B-O}/2) + d_{A^{II}-O3} \sin(\phi_{O3-A^{II}-O3}/2)]/[2 \cdot d_{A^{I}-O1}]. \quad (20)$$

Finally, by substituting (20) into (9), the lattice parameter a is determined from the following relationship

$$\begin{aligned} a = {} & 3^{1/2}\{d^2_{A^{I}-O1} - (1/4) \cdot [d_{B-O} \sin(\tau'_{O-B-O}/2) \\ & + d_{A^{II}-O3} \sin(\phi_{O3-A^{II}-O3}/2)]^2\}^{1/2} \cos[(\pi/6) - \delta_{A^{I}} - \alpha_{A^{I}}] \\ & + 3^{1/2}\{(d_{A^{I}-O1} + \Delta_{A^{I}-O})^2 - (1/4) \cdot [d_{B-O} \sin(\tau'_{O-B-O}/2) \\ & + d_{A^{II}-O3} \sin(\phi_{O3-A^{II}-O3}/2)]^2\}^{1/2} \cos[(\pi/6) - \delta_{A^{I}} + \alpha_{A^{I}}] \\ & + 2(3^{1/2}) d_{B-O} \sin(\tau_{O-B-O}/2) \cos(\theta), \end{aligned} \quad (21a)$$

where

$$\begin{aligned} \sin(\theta) = {} & \{\{d^2_{A^{I}-O1} - (1/4) \cdot [d_{B-O} \sin(\tau'_{O-B-O}/2) \\ & + d_{A^{II}-O3} \sin(\phi_{O3-A^{II}-O3}/2)]^2\}^{1/2} \sin[(\pi/6) - \delta_{A^{I}} - \alpha_{A^{I}}] \\ & - \{(d_{A^{I}-O1} + \Delta_{A^{I}-O})^2 - (1/4) \cdot [d_{B-O} \sin(\tau'_{O-B-O}/2) \\ & + d_{A^{II}-O3} \sin(\phi_{O3-A^{II}-O3}/2)]^2\}^{1/2} \sin[(\pi/6) \\ & - \delta_{A^{I}} + \alpha_{A^{I}}]\}/[2d_{B-O} \sin(\tau_{O-B-O}/2)]. \end{aligned} \quad (21b)$$

This work was supported through the NRC/A*STAR Joint Research Programme on 'Advanced Ceramic Methods for the Co-stabilization and Recycling of Incinerator Fly Ash with Industrial Wastes'.

References

Akao, M., Aoki, H., Innami, Y., Minamikata, S. & Yamada, T. (1989). *Iyo Kizai Kenkyusho Hokoku, Tokyo Ika Shika Daigaku*, **23**, 25–29.

Alberius-Henning, P., Mattsson, C. & Lidin, S. (2000). *Z. Kristallogr.* **215**, 345–346.

Alberius-Henning, P., Moustiakimov, M. & Lidin, S. (2000). *J. Solid State Chem.* **150**, 154–158.

Belokoneva, E. L., Troneva, E. A., Demýanets, L. N., Duderov, N. G. & Below, N. V. (1982). *Kristallografiya*, **27**, 793–794.

Bigi, A., Ripamonti, A., Brückner, S., Gazzano, M., Roveri, N. & Thomas, S. A. (1989). *Acta Cryst.* B**45**, 247–251.

Boer, B. G. de, Sakthivel, A., Cagle, J. R. & Young, R. A. (1991). *Acta Cryst.* B**47**, 683–692.

Calos, N. J. & Kennard, C. H. L. (1990). *Z. Kristallogr.* **191**, 125–129.

Carrillo-Cabrera, W. & von Schnering, H. G. (1999). *Z. Anorg. Allg. Chem.* **625**, 183–185.

Chen, X., Wright, J. V., Conca, J. L. & Peurrung, L. M. (1997). *Water Air Soil Pollut.* **98**, 57–78.

Christy, A. G., Alberius-Henning, P. & Lidin, S. A. (2001). *J. Solid State Chem.* **156**, 88–100.

Crannell, B. S., Eighmy, T. T., Krzanowski, J. E., Eusden, J. D. Jr, Shaw, E. L. & Francis, C. A. (2000). *Waste Manag.* **20**, 135–148.

Comodi, P., Liu, Y., Zanazzi, P. F. & Montagnoli, M. (2001). *Phys. Chem. Miner.* **28**, 219–224.

Corker, D. L., Chai, B. H. T., Nicholls, J. & Loutts, G. B. (1995). *Acta Cryst.* C**51**, 549–551.

Dai, Y. & Hughes, J. M. (1989). *Can. Mineral.* **27**, 189–192.

Dai, Y., Hughes, J. M. & Moore, P. B. (1991). *Can. Mineral.* **29**, 369–376.

Dardenne, K., Vivien, D. & Huguenin, D. (1999). *J. Solid State Chem.* **146**, 464–472.

Davidson, E. R. (1983). *Methods in Computational Molecular Physics*, Vol. 113, *NATO Advanced Study Institute, Series C*, edited by G. H. F. Diercksen and S. Wilson, p. 95. New York: Plenum Press.

Donnay, J. D. H. & Ondik, H. (1972–1983). Editors. *Crystal Data Determinative Table*s, 6 volumes. US Department of Commerce, National Bureau of Standards, Washington, DC, USA.

Dong, Z. & White, T. J. (2004*a*). *Acta Cryst.* B**60**, 138–145.

Dong, Z. & White, T. J. (2004*b*). *Acta Cryst.* B**60**, 146–154.

Dong, Z., White, T. J., Wei, B. & Laursen, K. (2002). *J. Am. Ceram. Soc.* **85**, 2515–2522.

Eighmy, T. T., Crannell, B. S., Krzanowski, J. E., Butler, L. G., Cartledge, F. K., Emery, E. F., Eusden, J. D. Jr, Shaw, E. L. & Francis, C. A. (1998). *Waste Manag.* **18**, 513–524.

Elliott, J. C. (1994). *Structure and Chemistry of the Apatites and other Calcium Orthophosphates.* Amsterdam: Elsevier.

Elliot, J. C., Dykes, E. & Mackie, P. E. (1981). *Acta Cryst.* B**37**, 435–438.

Felsche, J. (1972). *J. Solid State Chem.* **5**, 266–275.

Ferraris, C., White, T. J., Plévert, J. & Wegner, R. (2005). *Phys. Chem. Miner.* **32**, 485–492.

Hashimoto, H. & Matsumoto, T. (1998). *Z. Kristallogr.* **213**, 585–590.

Hata, M., Marumo, F., Wai, S. & Aoki, H. (1979). *Acta Cryst.* B**35**, 2382–2384.

Hawthorne, F. C. (1994). *Acta Cryst.* B**50**, 481–510.

Ioannidis, T. A. & Zouboulis, A. I. (2003). *J. Hazard. Mater. B*, **97**, 173–191.

Ivanov, A., Simonov, M. A. & Belov, N. (1976). *Zh. Strukt. Khim.* **17**, 375–378.

Kim, J. Y. (2001). PhD dissertation. School of Chemistry, The University of Sydney, Australia.

Kim, J. Y., Dong, Z. & White, T. J. (2005). *J. Am. Ceram. Soc.* **88**, 1253–1260.

Kim, J. Y., Fenton, R. R., Hunter, B. A. & Kennedy, B. J. (2000). *Aust. J. Chem.* **53**, 679–686.

Kohn, M. J., Rakovan, J. & Hughes, J. M. (2002). Editors. *Phosphates: Geochemical, Geobiological, and Materials Importance. Reviews in Mineralogy and Geochemistry*, Vol. 48. Mineralogical Society of America, Washington, DC, USA.

Kresse, G. (1993). PhD thesis. Technische Universita Wien, Austria.

Kresse, G. & Hafner, J. (1993). *Phys. Rev. B*, **48**, 13115–13118.

Kresse, G. & Hafner, J. (1994). *Phys. Rev. B*, **49**, 14251–14269.

Kresse, G. & Joubert, J. (1999). *Phys. Rev. B*, **59**, 1758–1775.

Le Page, Y. & Rodgers, J. (2005). *J. Appl. Cryst.* **38**, 697–705.

Le Page, Y., Saxe, P. & Rodgers, J. (2002). *Acta Cryst.* B**58**, 349–357.

Mackie, P. E. & Young, R. A. (1973). *J. Appl. Cryst.* **6**, 26–31.

Majid, C. A. & Hussain, M. A. (1996). *Proc. Pakistan Acad. Sci.* **33**, 11–17.

Mathew, M., Mayer, I., Dickens, B. & Schroeder, L. W. (1979). *J. Solid State Chem.* **28**, 79–95.

McConnell, D. (1973). *Apatite. Its Crystal Chemistry, Mineralogy, Utilization and Geologic and Biologic Occurrences.* New York, USA: Springer.

Methfessel, M. & Paxton, A. T. (1989). *Phys. Rev. B*, **40**, 3616–3621.

Monkhorst, H. J. & Pack, J. D. (1976). *Phys. Rev. B*, **13**, 5188–5192.

Nötzold, D. & Wulff, H. (1998). *Powder Diffr.* **13**, 70–73.

Nötzold, D., Wulff, H. & Herzog, G. (1994). *J. Alloys Compds*, **215**, 281–288.

Pan, Y. & Fleet, M. E. (2002). *Phosphates: Geochemical, Geobiological, and Materials Importance*, Vol. 48, *Reviews in Mineralogy and Geochemistry*, edited by M. J. Kohn, J. Rakovan & J. M. Hughes, pp. 13–49. Mineralogical Society of America, Washington, DC, USA.

Rouse, R. C., Dunn, P. J. & Peacor, D. R. (1984). *Am. Mineral.* **69**, 920–927.

Saenger, A. T. & Kuhs, W. F. (1992). *Z. Kristallogr.* **199**, 123–148.

Slater, P. R., Sansom, J. E. H. & Tolchard, J. R. (2004). *Chem. Rec.* **4**, 373–384.

Sudarsanan, K. & Young, R. A. (1974). *Acta Cryst.* B**30**, 1381–1386.

Sudarsanan, K., Young, R. A. & Donnay, J. D. H. (1973). *Acta Cryst.* B**29**, 808–813.

Sudarsanan, K., Mackie, P. E. & Young, R. A. (1972). *Mater. Res. Bull.* **7**, 1331–1338.

Trotter, J. & Barnes, W. H. (1958). *Can. Mineral.* **6**, 161–173.

Valsami-Jones, E., Ragnarsdottir, K. V., Putnis, A., Bosbach, D., Kemp, A. J. & Gressey, G. (1998). *Chem. Geol.* **151**, 215–233.

White, T. J., Ferraris, C., Kim, J. & Madhavi, S. (2005). *Apatite – An Adaptive Framework Structure*, in *Reviews in Mineralogy and Geochemistry*, Vol. 57, *Micro- and Mesoporous Mineral Phases*, edited by G. Ferraris & S. Merlino, pp. 307–373. Mineralogical Society of America and Geochemical Society, Washington, DC, USA.

White, T. J. & Dong, Z. (2003). *Acta Cryst.* B**59**, 1–16.

Zhang, P. & Ryan, J. A. (1999). *J. Environ. Sci. Technol.* **33**, 625–630.